

# Photometric observations of NGC 281: Detection of 228 variable stars

Sneh Lata<sup>1\*</sup>, A. K. Pandey<sup>1</sup>, J. C. Pandey<sup>1</sup>, Neelam Panwar<sup>1</sup>, Paulomi Paul<sup>1</sup>

<sup>1</sup>*Aryabhata Research Institute of Observational Sciences, Manora Peak, Nainital 263002, Uttarakhand, India*

Accepted ——. Received ——;

## ABSTRACT

We identify 228 periodic variables in the region of young open cluster NGC 281 using time series photometry carried out from 1 m class ARIES telescopes, Nainital. The cluster membership of these identified variables is determined on the basis colour-magnitude, two colour diagrams and kinematic data. Eighty one variable stars are found to be members of the cluster NGC 281. Of 81 variables, 30 and 51 are probable main-sequence and pre-main-sequence members, respectively. Present study classifies main-sequence variable stars into different variability types according to their periods of variability, shape of light curves and location in the Hertzsprung-Russell diagram. These identified main-sequence variables could be  $\beta$  Cep,  $\delta$  Scuti, slowly pulsating B type and new class variables. Among 51 pre-main-sequence variables, majority of them are weak line T Tauri stars. The remaining 147 variables could belong to the field population. The variability characteristics of the field population indicate that these variables could be RR Lyrae,  $\delta$  Scuti and binaries type variables.

**Key words:** Open cluster: NGC 281 – colour-magnitude diagram: Variables: pre-main-sequence stars; T Tauri stars

## 1 INTRODUCTION

This work presents time series observations of young open cluster NGC 281 as a part of our ongoing project entitled “Search for pre-main-sequence (PMS) variability in Young Open Clusters (YOCs)”. YOCs contain significant number of PMS stars with circumstellar disk and are unique laboratories to study the evolution of disks of PMS stars. In general, PMS stars are young low-mass sources which remain deeply embedded the parent molecular cloud. PMS stars show variability associated to a number of different physical processes. Most of the physical processes such as dark spots and flaring, etc are associated with magnetic and rotational activities (Herbst et al. 1994). As a result, PMS variability can be expressed over a wide range of timescales, from intra day to months. These PMS stars accrete matter from their surrounded accretion disk and show prominent features such large IR excess and  $H\alpha$  emission line. In addition to PMS stars, YOCs also contain several O, B and Be type stars which are also found to be pulsating or rotating variables with timescales that range from minutes to years. Among these variables, there are about 20% B-type stars which show Be phenomenon i.e. B star with emission line.

Be type variables are very rapidly rotating main-sequence (MS) stars surrounded by a circumstellar envelope of gas. These stars show variability which is related to the presence of a circumstellar disk of variable size and structure (Arcos et al. 2018).

NGC 281 is a basically HII region known as Sh2-184 and located at a distance of 2.8 kpc (Elmegreen & Lada 1978; Sato et al. 2008; Sharma et al. 2012). The MS of this cluster is well defined and contains significant number of O and B spectral type stars. The reddening  $E(B-V)$  towards the cluster is found to be low  $\sim 0.32$  mag. Previous studies suggest that star formation is still continued in this cluster, hence the cluster provides an excellent laboratory to search PMS for variable stars. A detailed multiwavelength study of the region containing NGC 281 was presented by Sharma et al. (2012). They found that the majority of the identified PMS stars have age  $\sim 1-2$  Myr and their masses range from  $0.5$  to  $3.5M_{\odot}$ . Recently, Ivers et al. (2014) examined mid and far infrared images of NGC 281 at 24, 70, 100, 160  $\mu\text{m}$  wavelength taken from the Herschel and Spitzer Space Observatories to understand the mechanisms of star formation. They found two different populations of protostars in the region of NGC 281. In the WEST of NGC 281, protostars are found to be within a large molecular cloud obscured by dust while other population of protostars is associated with

\* E-mail: sneh@aries.res.in

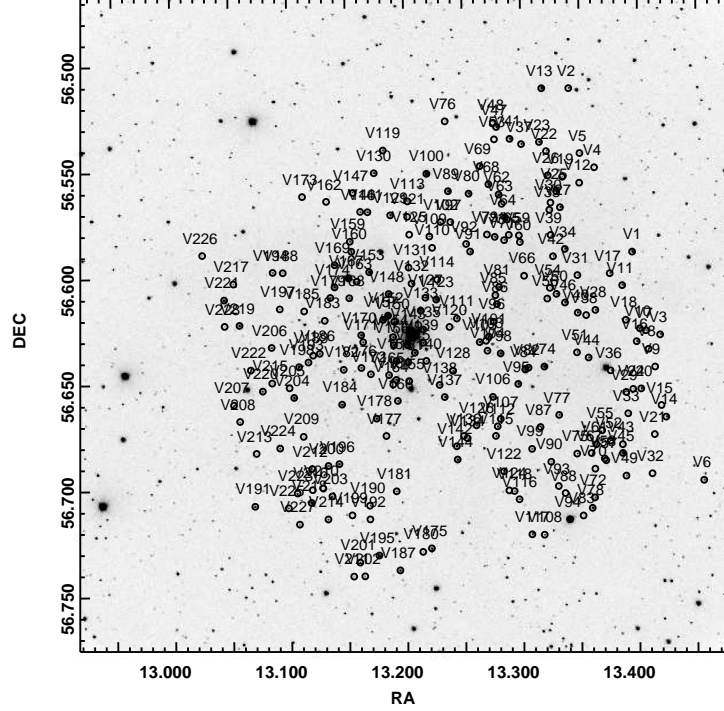


**Figure 1.** The observed image in  $V$  band which contains open cluster NGC 281. The stars detected as variables are encircled.

**Table 1.** Log of the observations. N and Exp. represent number of frames obtained and exposure time, respectively.

S. No.	Date of observations	Object	$V$ (N $\times$ Exp.)	$I$ (N $\times$ Exp.)
1	28 Oct 2010	NGC 281	4 $\times$ 50s	4 $\times$ 30s
2	30 Oct 2010	NGC 281	4 $\times$ 10s, 60s, 200s, 300s	10s, 40s, 150s
2	30 Oct 2010	SA 98	2 $\times$ 50s, 15s	2 $\times$ 30s, 10s, 50s
3	28 Nov 2011	NGC 281	3 $\times$ 50s	-
4	01 Dec 2011	NGC 281	80 $\times$ 50s	-
5	02 Dec 2011	NGC 281	84 $\times$ 50s	-
6	06 Dec 2012	NGC 281	80 $\times$ 50s	-
7	08 Dec 2012	NGC 281	51 $\times$ 50s	-
8	24 Oct 2014	NGC 281	164 $\times$ 40s	3 $\times$ 50s
9	25 Oct 2014	NGC 281	147 $\times$ 40s	-
10	24 Nov 2014	NGC 281	112 $\times$ 50s	-
11	23 Dec 2014	NGC 281	105 $\times$ 50s	-
12	27 Oct 2017	NGC 281	70 $\times$ 40s	-
13	10 Nov 2017	NGC 281	139 $\times$ 40s	-

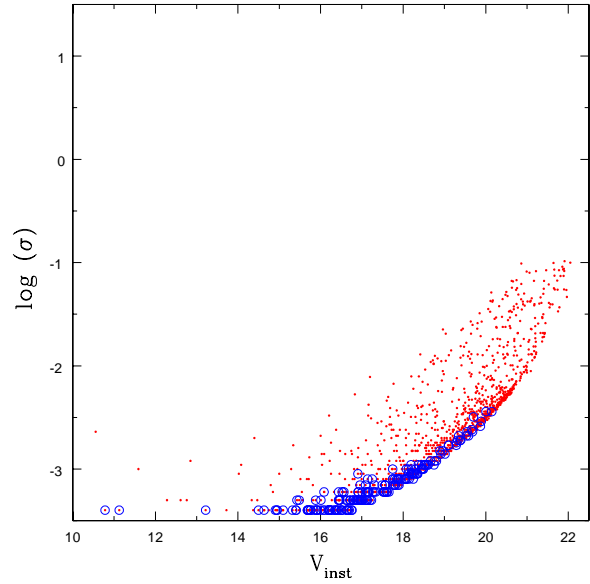


**Figure 2.** Photometric errors as a function of magnitude. Open circles represent the variables stars identified in the present work.

filamentary pillars and triggered star formation in the East of NGC 281.

We present time series data of stars in the region of the cluster NGC 281. The observations of the field containing NGC 281 were initiated in October 2010 and continued till November 2017. Section 2 describes observations, reduction procedure, comparison of different photometries, variable identification and period determination. Section 3 deals with membership of stars whereas the nature of variable stars identified in the present work has been discussed in section 4. Finally in section 5, we summarize our results.

## 2 OBSERVATIONS AND DATA REDUCTION

Time series  $V$  and  $I$  band observations of NGC 281 were obtained using a  $2048 \times 2048$  pixel CCD camera which is mounted at the f/13 Cassegrain focus of the 1.04-m ARIES Telescope, Nainital, India. The CCD with a plate scale of

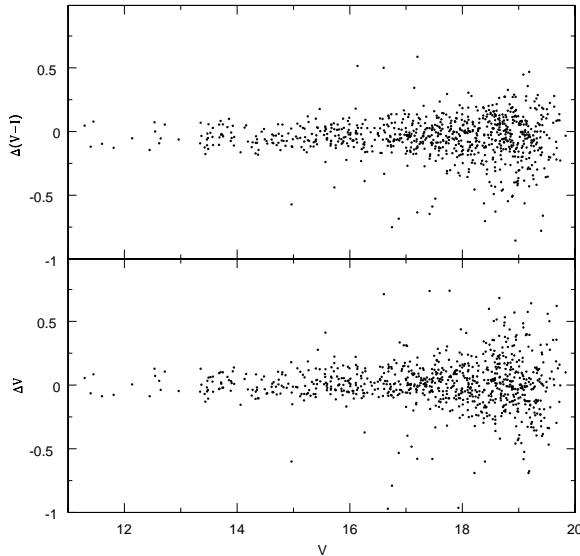


**Figure 3.** Comparison of the present and previous (Sharma et al. 2012). The  $\Delta$  represents the difference (present-previous photometry) between the two photometries.

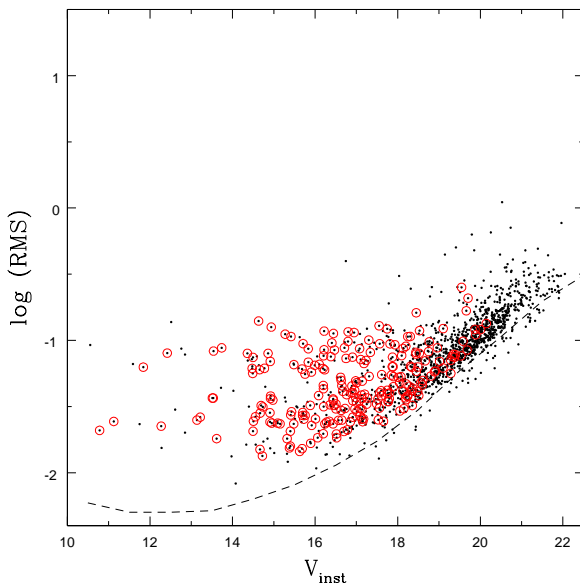


**Figure 4.** Magnitude as a function of standard deviation of each star detected in the present photometry in  $V$  band. Open circles represent variable stars identified in the work. The dashed line shows median magnitude scatter expected from the individual standard errors in different magnitude bins.

0.37 arcsec/pixel covers a field of about  $13 \times 13$  arcmin<sup>2</sup> on the sky. The observations were carried out in a binning mode of  $2 \times 2$  pixels in order to improve the signal-to-noise ratio. During the observations the seeing was around 2 arcsec. To standardize the observations, the SA 98 field of Landolt (1992) was also observed. A number of bias and twilight flat frames were also taken during the observations.

The  $V$  band optical observations of NGC 281 were also

performed on 27 October 2017 and 10 November 2017 from 1.30-m ARIES Devasthal optical telescope, Nainital, India. This telescope is equipped with  $2048 \times 2048$  pixel<sup>2</sup> CCD camera with a plate scale 0.54 arcsec per pixel, which gives field of view about 18 arcmin $\times$ 18 arcmin.

A total of 1046 and 10 observations of the cluster region were secured in  $V$  and  $I$  bands on 13 and 3 nights, respectively. The log of observations is given in Table 1. Fig. 1 shows the observed image in  $V$  band from 1.30-m ARIES Devasthal optical telescope. The observed images were preprocessed using tasks zerocombine, flatcombine and CCDPROC available in the IRAF<sup>1</sup> software package. The DAOPHOT package (Stetson 1987) was used to estimate the instrumental magnitudes. To construct the point spread function (PSF) of images isolated stars across the observed field were selected. The PSF photometry of all the sources was obtained using the ALLSTAR task. DAOMATCH (Stetson 1992) routine of DAOPHOT was used to match up observations taken on various nights with different telescopes. It finds the translation, rotation and scaling solutions between different photometry files, whereas DAOMASTER (Stetson 1992) takes .mch file given by DAOMATCH to match the point sources. DAOMASTER corrects all magnitudes for each star to the magnitude scale of the reference frame. The instrumental magnitudes were translated to the standard magnitudes using the observations of Landolt SA98 standard stars (Landolt 1992). We derived the transformation equations which includes the zero points and colour coefficients as

$$v = V + a_1 - b_1 \times (V - I) + 0.25 \times X$$

$$i = I + a_2 - b_2 \times (V - I) + 0.10 \times X$$

where  $v$  and  $i$  are the instrumental magnitudes and  $X$  is the airmass. The values of  $a_1$ ,  $a_2$ ,  $b_1$ , and  $b_2$  are found to be  $5.4148645 \pm 0.0037297$ ,  $5.6550550 \pm 0.0021983$ ,  $0.0379665 \pm 0.0031046$ , and  $0.0433376 \pm 0.0017998$  respectively.

The standard photometric error of the mean magnitude for each star, based on photometric error of individual frame, has been taken from the .mag file generated by the DAOMASTER. The estimated photometric error of all the stars as a function mean instrumental magnitude is shown in Fig. 2.

## 2.1 Comparison with Previous Photometry

The present CCD photometric data have been compared with the CCD observations given by Sharma et al. (2012). We have found 867 common stars between these two photometries. The difference  $\Delta$  (present data - literature data) as a function of  $V$  magnitude is shown in Fig. 3, which indicates that the present  $V$  magnitudes are in agreement with those given by Sharma et al. (2012), whereas a systematic difference of 0.05 mag in  $(V - I)$  colour is present between the two photometries.

<sup>1</sup> IRAF is distributed by the National Optical Astronomy Observatory, which is operated by the Association of Universities for Research in Astronomy (AURA) under cooperative agreement with the National Science Foundation

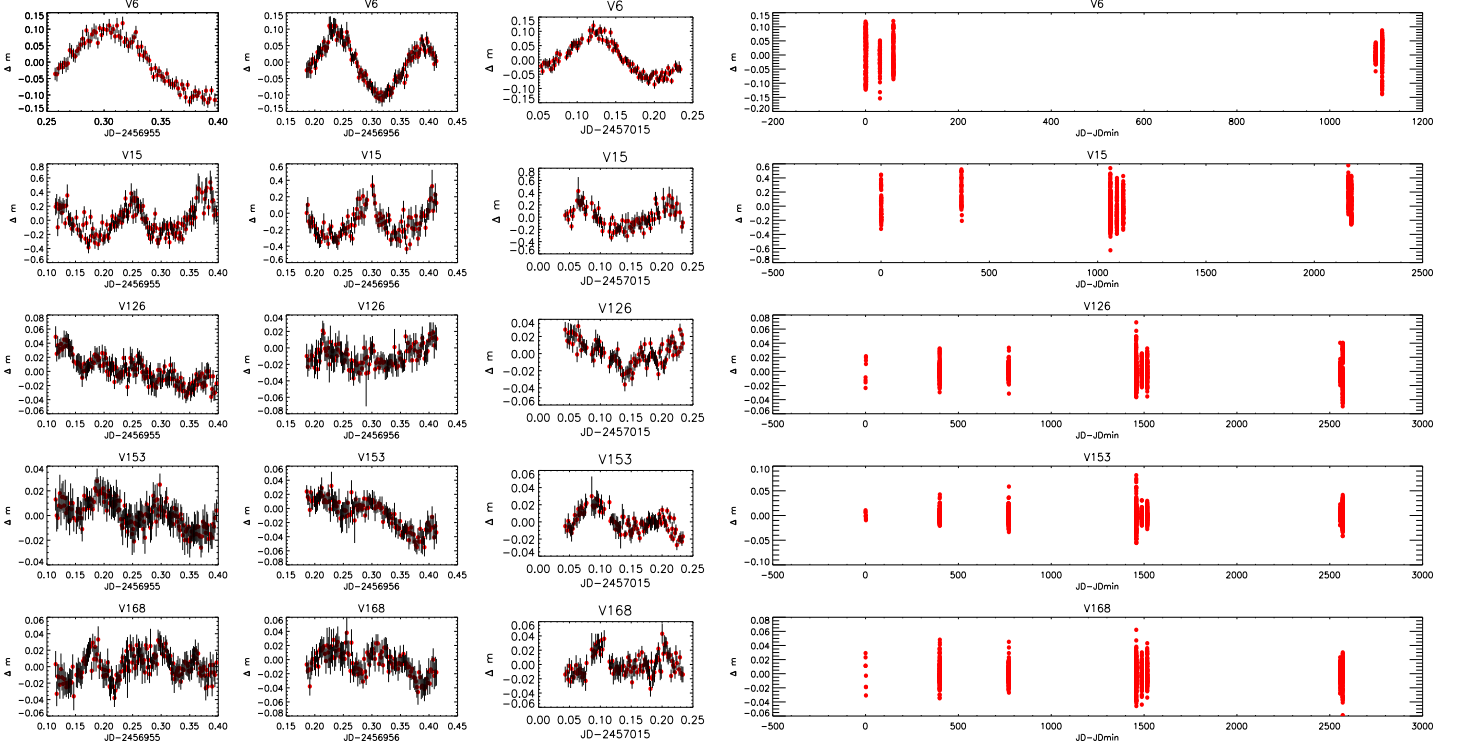


**Figure 5.** The V band sample light curves of a few variables identified in the present work where  $\Delta m$  represents the differential magnitude. The individual night observations of stars are shown in left panel while right panel represents all the observations of stars. The complete Figure 5 is available in electronic form.

## 2.2 Variables identification

The differential magnitudes ( $\Delta m$ ) in the sense variable minus comparison star were plotted against Julian date (JD). To obtain differential magnitude of target star (V), we have selected three non variable stars C1, C2 and C3 as comparison stars in the field of NGC 281. Then, magnitude difference V-C1, C1-C2, C1-C3 have been determined relative to C1. The comparison stars C2 and C3 have been used to check non variable nature of C1. The probable variables were identified visually by inspecting the light curves. The visual inspection yielded 228 variable candidates. In order to verify variability of these stars, *rms* (root mean square) scatter is computed for each star. The observed *rms* scatter includes both the intrinsic variability and the mean photometric error. In Fig. 4 we have plotted *rms* of each observed star as a function of magnitude, where open circles show the variables identified in the present work. Fig. 4 indicates that generally identified variables have higher *rms* value. The lower *rms* stars in general are low amplitude variables. There are 4 variables with *rms* > 3 times the mean *rms* of the magnitude bin. Ten and 48 variables have *rms* > 2 times the mean *rms* of the magnitude bin and *rms* > 1 times the mean *rms* of the magnitude bin, respectively. The light curves of some of the stars having large *rms* do not show any variability. These stars are either having some outliers or located on edge of CCD frame. Low amplitude variables have been detected visually by inspecting their light curves. The photometric variability of stars identified as variables has also been checked using the *Chi* square test (Sesar et al. 2007). All 228 variables have probability  $\geq 90\%$  except four

stars V129, V136, V139, V141 and V146 for which probability to be a variable is less than 90%. We considered these stars as variable on the basis of visual inspection of their light curves. The sample light curves of a few variables are shown in Fig 5. The identification number, coordinates and optical data for these variable stars are given in Table 2. The CCD pixel coordinates of these identified variables were converted to celestial coordinates (RA and DEC) for J2000 with the help of the CCMAP and CCTRAN tasks in IRAF. The reference astrometric catalog was made from DSS2 R band image (<https://skyview.gsfc.nasa.gov/current/cgi/query.pl>) which was used in CCMAP to determine the plate solution for the image. The variable candidates identified in the present work are marked in Fig. 1.

To determine periods of variable stars we applied the Lomb-Scargle (LS) periodogram (Lomb 1976; Scargle 1982). This periodogram is known to work well if data are unevenly sampled. The false alarm probabilities corresponding to the power of maximum frequency from LS for all the identified variables come out to be zero. The peak of the periodogram ranges from 0.076 to 0.92 for variable stars. The range of highest periodogram peak for the present variables is between  $\sim 0.021$  to  $\sim 0.038$ ,  $\sim 0.023$  to  $\sim 0.040$  and  $\sim 0.026$  to  $\sim 0.046$  at 10%, 5% and 1% false alarm probabilities, respectively. The light curves of stars were folded with calculated period. We visually inspected the phased light curves and opted for the period showing the best phased light curve. The most probable periods with amplitude are listed in Table 2. The phased light curves of periodic and semi periodic/irregular variables candidates are shown in Fig. 6 and



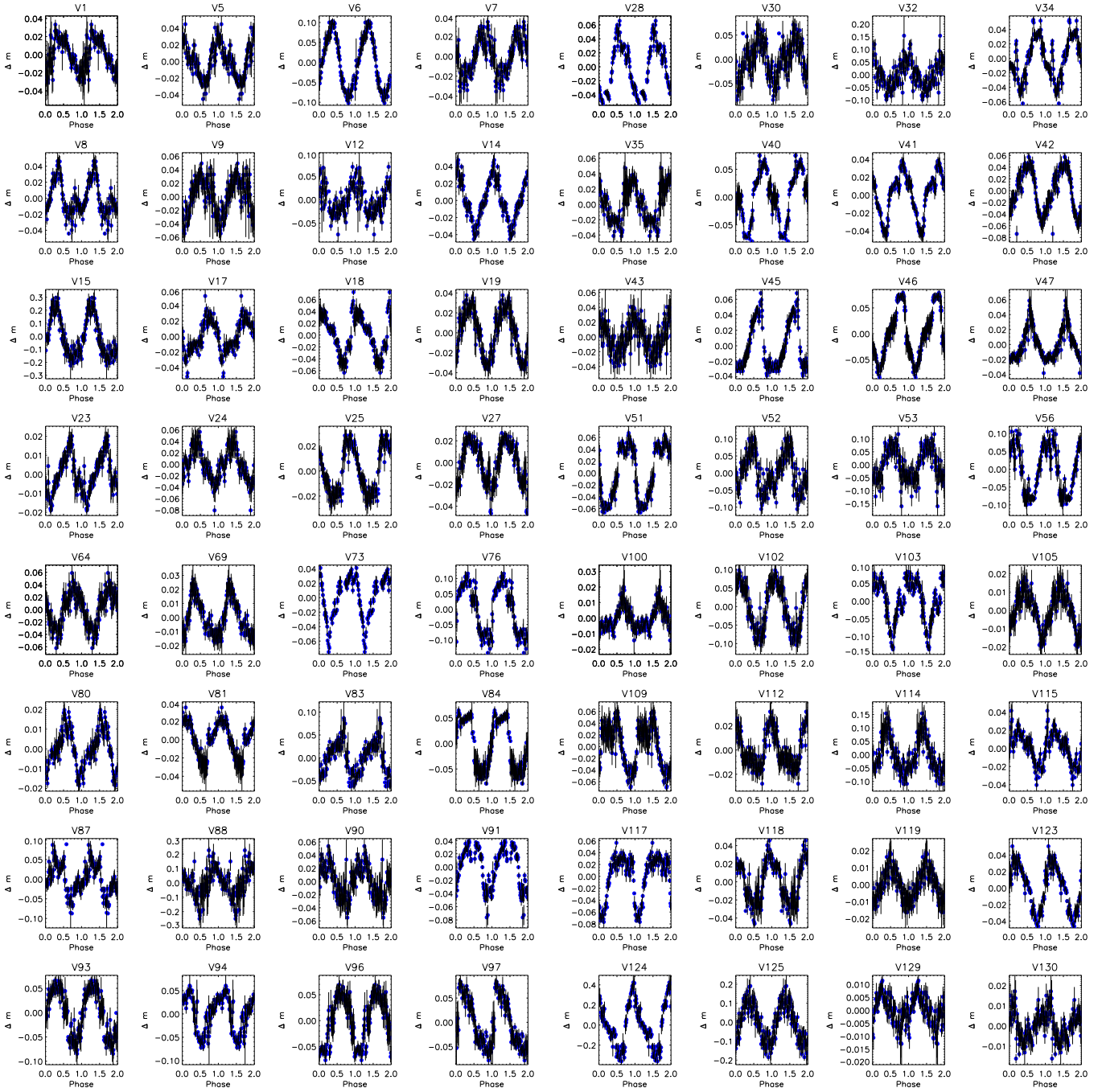


**Figure 6.** The V band phased light curves of periodic variable stars.

Fig. 7, respectively where averaged differential magnitude in 0.02 phase bin along with  $\sigma$  error bar has been plotted. A few of the individual data points which show relatively large photometric errors have not been considered in folding the light curves. During calculation of period for short period variable stars, if there was a vertical shift between the observations for different nights, it was calculated and applied to bring different night observations at same level. In the present study several stars seem to have many periods. These could be semi periodic/irregular variables (light curves shown in Fig. 7). The light curves of these stars were

folded with their best periods as folded data with the best period gives smooth phased light curve of the star. These irregular/semiperiodic variables could be binary systems with pulsating components with multiple periods or other complex systems. From now, we have considered them as probable periodic variable stars. The phased light curves will be further discussed in Section 7.

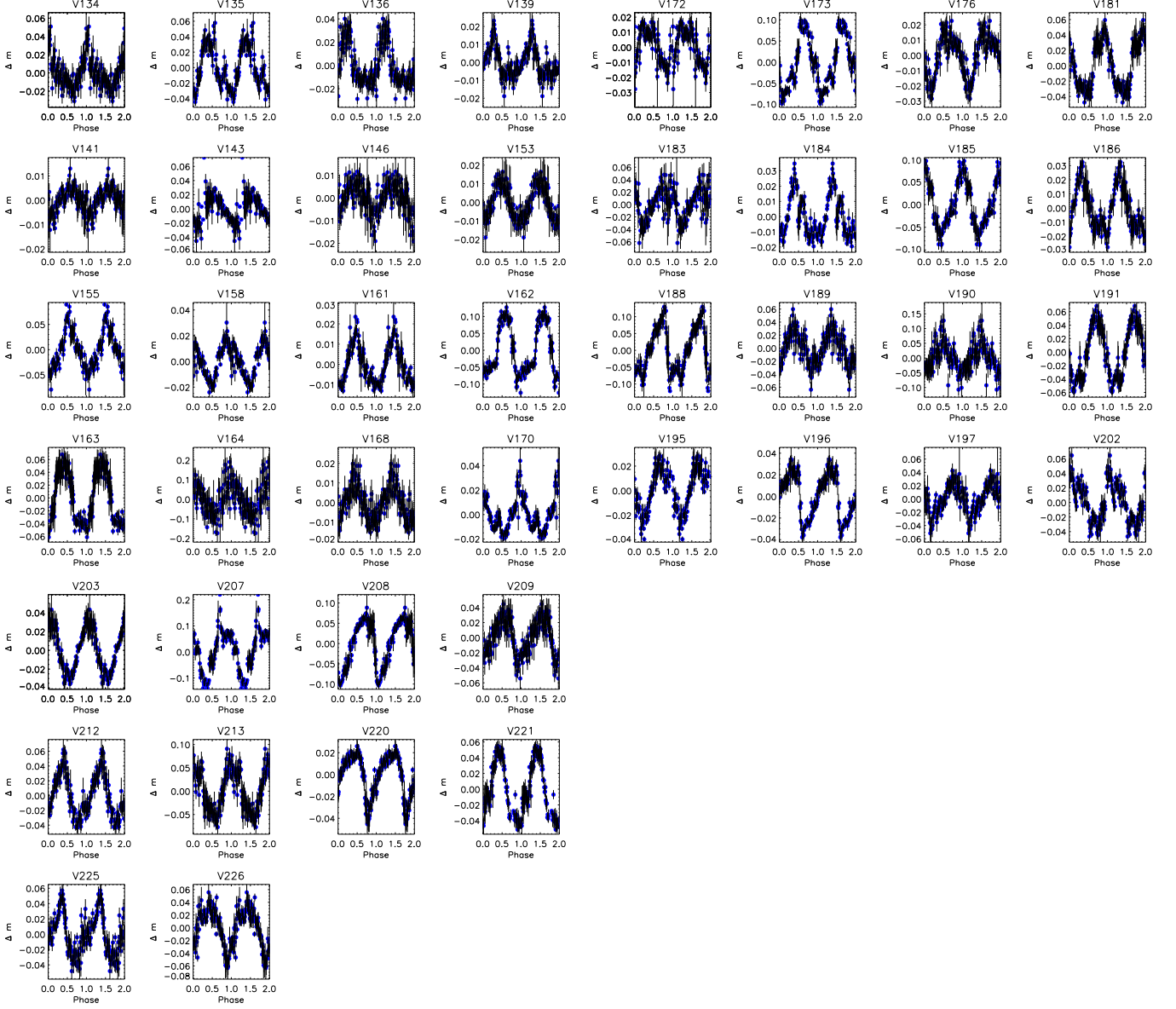


Figure 6. Continued.

### 3 CLUSTER MEMBERSHIP OF THE IDENTIFIED VARIABLES

The characterization of the identified variables needs information whether these are the members of the cluster or not. The *UBVI* (*UBV* data taken Sharma et al. 2012 and present *VI* data) and *JHK* photometric observations of the cluster NGC 281 (Cutri et al. 2003) have been used to establish the membership of the identified variables. In addition, the membership of a star is also verified with the help of proper motion data taken from Gaia astrometric mission (Gaia Collaboration et al. 2018)

#### 3.1 *U* - *B*/*B* - *V* Two colour diagram (TCD)

The *U* - *B*/*B* - *V* TCD is a useful tool to identify MS members of the cluster region. The *U* - *B* data for only 128 identified variables are available in Sharma et al. (2012). Fig. 8 plots *U* - *B*/*B* - *V* TCD for 128 variables where the continuous curves show ZAMS from Girardi et al. (2002), which are shifted along the reddening vector having a slope of  $E(U - B)/E(B - V) = 0.72$ . The distribution of MS variables reveals a variable reddening in the cluster region with a minimum reddening  $E(B - V) = 0.32$  mag. The sources lying within the MS band having  $E(B - V) = 0.32$  mag

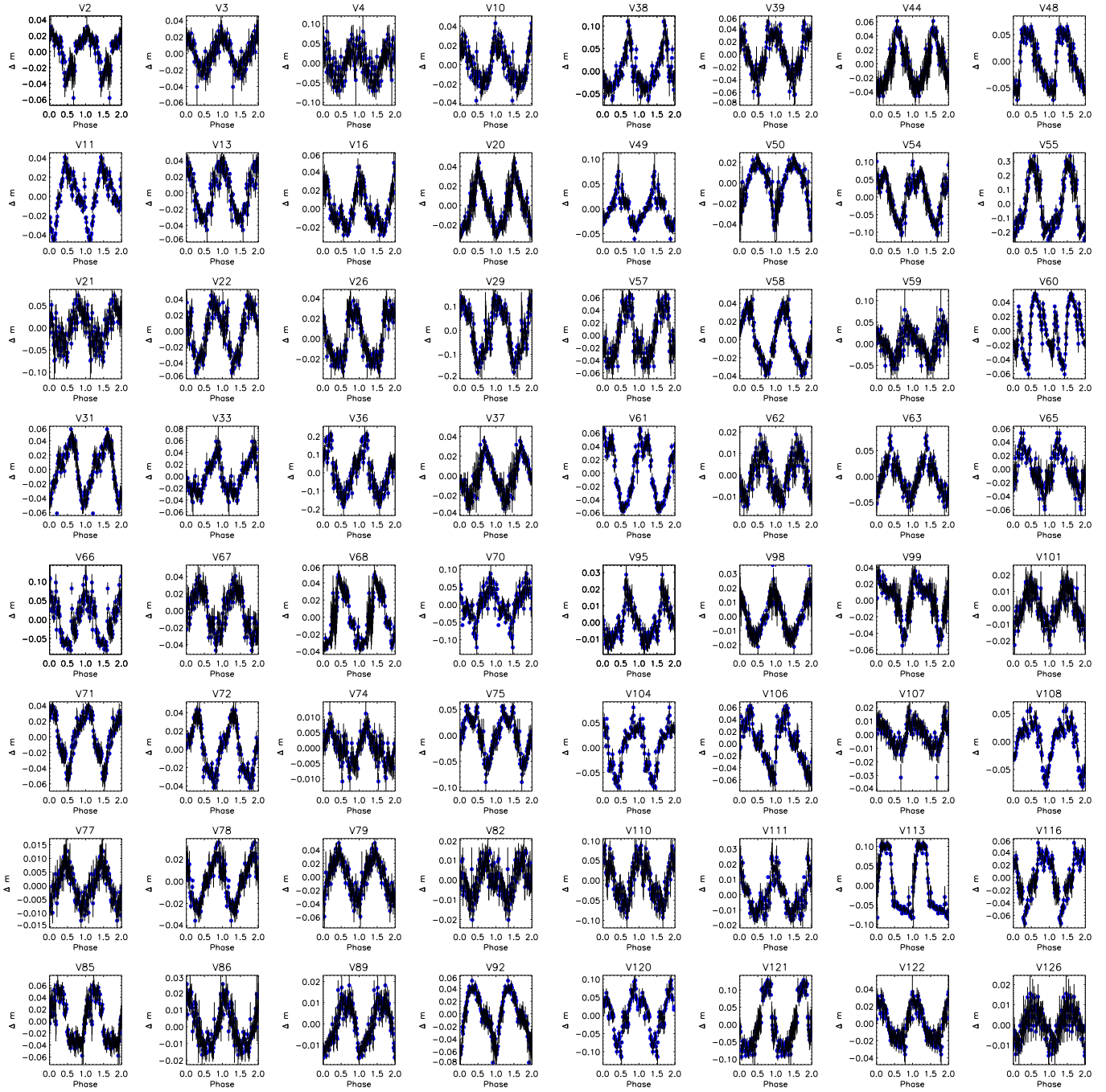


**Figure 7.** The V band phased light curves of probable periodic variable stars.

to 0.45 mag with O to A spectral type can be considered as possible MS members of the cluster. The identification as well as estimation of reddening for YSOs is not possible using the  $U - B/B - V$  TCD because the  $U$  and  $B$  band fluxes may be affected by excess due to accretion. Probable MS cluster members are mentioned in Table 2.

### 3.2 J-H/H-K TCD

Since young stellar objects (YSOs) generally show  $H\alpha$  emission, NIR excess or X-ray emission, therefore  $J -$

$H/H - K$  TCD is one of the very useful tools to identify PMS objects. Fig. 9 displays  $J - H/H - K$  TCD for all the identified variables.  $JHK$  data have been taken from the 2MASS catalogue (Cutri et al. 2003) which was further converted to CIT system using the relations given in the 2MASS website (<http://www.astro.caltech.edu/jmc/2mass/v3/transformations/>). In Fig. 9, the sources lying in ‘F’ region could be either field stars or Class III (WTTSs) and Class II (CTTSs) sources with small NIR excesses. The sources lying in the ‘T’ region can be considered mostly as Class II objects/ CTTSs (for detail, Lata et al.

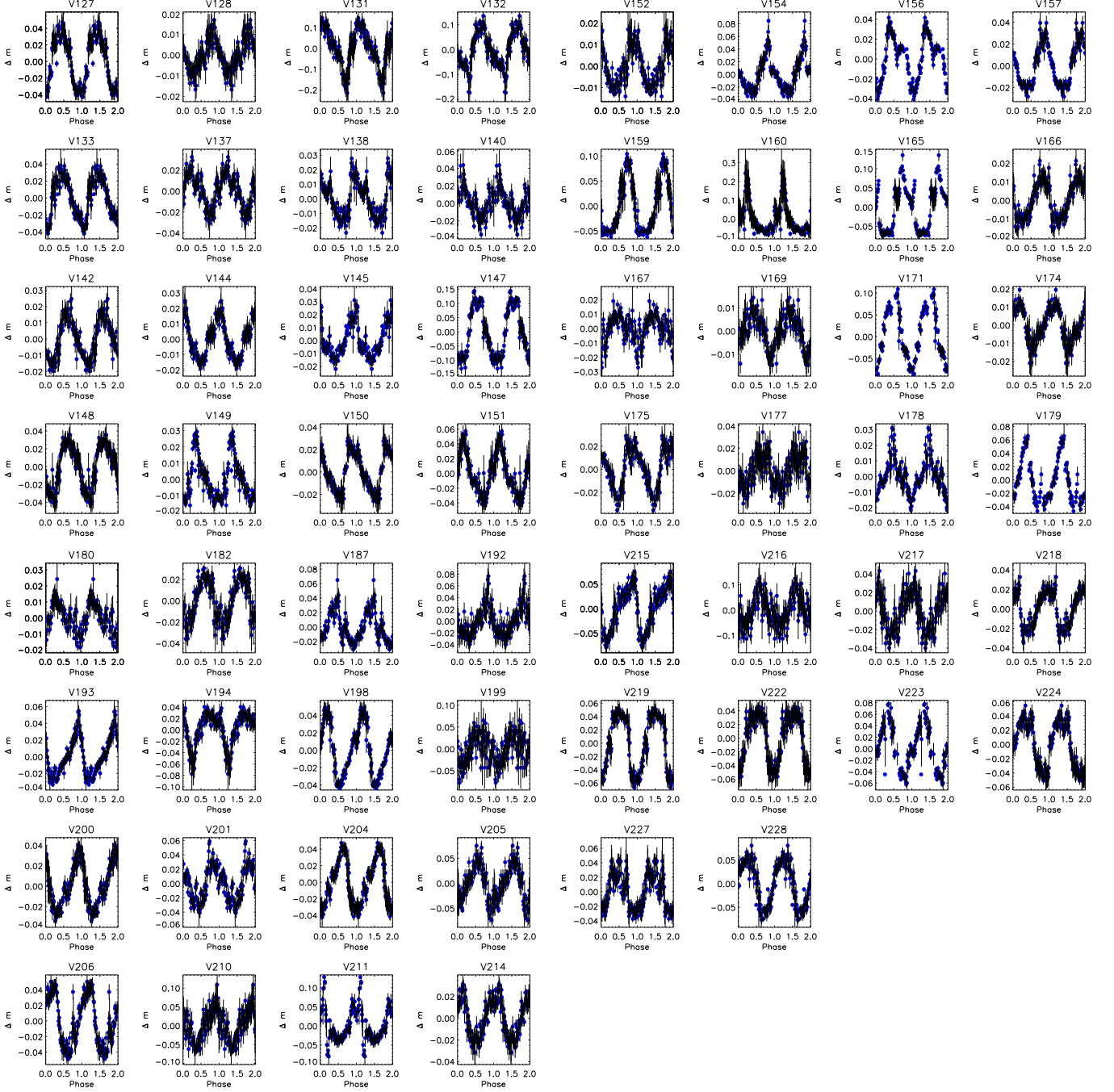
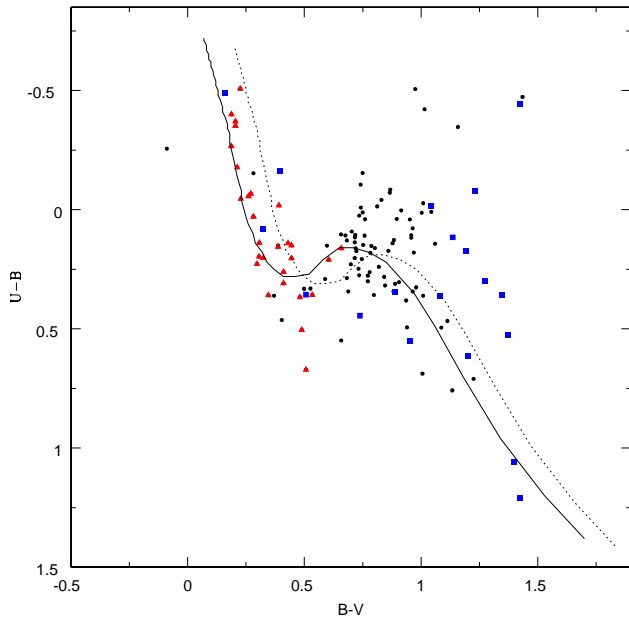


Figure 7. Continued.

2019). A comparison of the TCD of the NGC 281 region with the NIR TCD of nearby reference region (figure 6 of Sharma et al. 2012) indicates that the sources lying in the ‘F’ region above the extension of the intrinsic CTTS locus as well as sources having  $(J - H) \gtrsim 0.6$  mag and lying to the left of the first (left-most) reddening vector could be WTTs/Class III sources. Sharma et al. (2012) have also identified YSOs on the basis of  $H\alpha$  emission, NIR TCD, MIR TCD, and X-ray emission. A comparison of present data with that by Sharma et al. (2012) yields 11 common PMS stars. The MIR observations are very useful, which provide information of YSOs

remained embedded in the molecular clouds. Several studies (Getman et al. 2012; Jose et al. 2013) classify YSOs with help of MIR TCDs. In the IRAC colour plane, YSOs occupy distinct regions according to their nature. The figure 7 of Sharma et al. (2012) presents a  $[5.8]-[8.0]$  versus  $[3.6]-[4.5]$  TCD for the observed sources. This figure shows that class II, III and 0/I sources have different locations in these TCDs. The common YSOs are V76, V102, V103, V114, V133, V152, V156, V164, V171, V188 and V209. In  $J - H/H - K$  TCD star V152 lies below the intrinsic locus of T Tauri stars and right of middle reddening vector. Out of these 11 stars two





**Figure 8.**  $(U - B)/(B - V)$  TCD for variable stars identified in the present study. All the  $UBV$  data are taken from Sharma et al. (2012). The continuous and dotted line represent the ZAMS (Girardi et al. 2002) which are shifted along the reddening vector for reddening  $E(B - V) = 0.32$  mag and 0.45 mag. Triangles are identified as MS variables and filled squares show PMS variables.

sources V133 and V156 are found to be lying in the location of Herbig Ae/Be stars in  $J - H/H - K$  TCD. Details of the probable PMS cluster members are mentioned in Table 2.

### 3.3 V/V-I CMD

The  $V/V - I$  CMD for 225 identified variables is displayed in Fig. 10. The  $V - I$  colours for three variables were not available. The zero-age main-sequence (ZAMS) by Girardi et al. (2002) as well as PMS isochrones for various ages and evolutionary tracks for various masses by Siess et al. (2000) have also been plotted. Assuming the reddening  $E(V - I)$  towards the cluster as 0.40 mag, the comparison of observations with the ZAMS by Girardi et al. (2002) yields a distance modulus of 13.25 mag, which corresponds a distance of 2.82 kpc, which is in good agreement with the value (2.81 kpc) used by Sharma et al. (2008). The probable MS, PMS variables identified on the basis of CMD are shown with triangle and filled square symbols in Fig. 10, respectively. The variables having membership probabilities  $\geq 50\%$  (see next section) are encircled. Based on the above mentioned TCDs and CMD, we have established membership of 81 stars, of which 30 and 51 stars could be probable MS and PMS variables, respectively. Remaining 147 variables may belong to the field region. The classification of variables is given in the last column of Table 2.

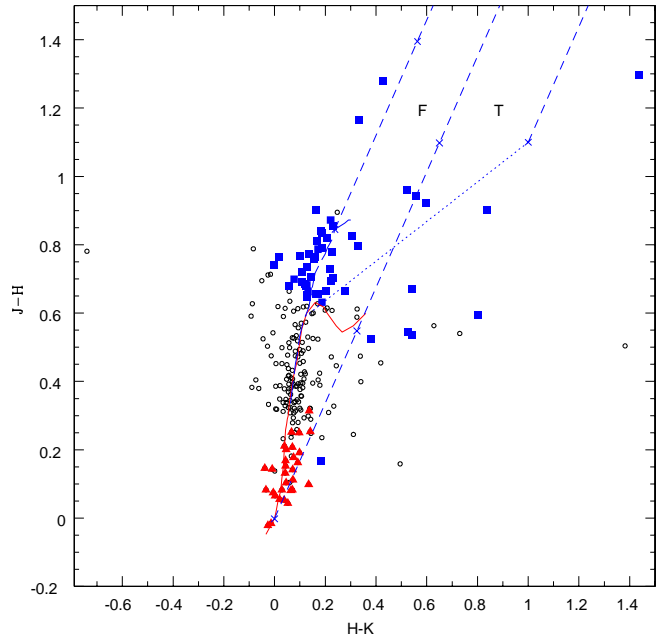


**Figure 9.**  $(J - H)/(H - K)$  TCD for variable stars detected in the field of NGC 281. The  $JHK$  data have been taken from the 2MASS catalogue (Cutri et al. 2003). The continuous and long dashed line show sequences for dwarfs and giants (Bessell & Brett 1988), respectively. The TTSs locus (Meyer et al. 1997) is shown by dotted line. The small dashed lines are reddening vectors (Cohen et al. 1981) and an increment of visual extinction of  $A_V = 5$  mag is denoted by crosses on the reddening vectors. Filled squares and triangles represent PMS and MS whereas open circles may be either MS members of the cluster or field stars. The ‘F’ and ‘T’ regions are explained in Section 3.2.

### 3.4 Kinematic data

The proper motion values of stars have been taken from Gaia astrometric mission (Gaia Collaboration et al. 2018). For this we have taken data of stars which lie within radial distance of 16 arcmin from center of the cluster NGC 281. The center of the cluster is assumed at RA=00h 52m 49s and Dec=56d 37m 48s (Sharma et al. 2012). For the membership probabilities of these stars, we used the online Clusterix membership (<http://clusterix.cerit-sc.cz/>) estimation tool which uses the Non-Parametric method for the cluster-field separation in 2-dimensional proper motion space. This approach uses the kernel estimation technique using a circular Gaussian kernel function to derive the data distributions as described by Cabrera-Cano & Alfaro (1990). The fundamental idea underlying this approach is the empirical determination of the cluster and field star distributions without any assumption regarding their shape. The non-parametric method works best for the open clusters where it is somewhat difficult to locate the center of the field region. The proper motion cut-off was set to 15 mas/yr and radius of the cluster was considered as 8.0 arcmin. For field region we have considered a region lying between 8 and 16 arcmin. Clusterix gave membership probabilities of 3748 stars. The cross matched between present data and data (proper motions and membership probabilities of stars) given by Clusterix reveals that 223 identified variables have membership



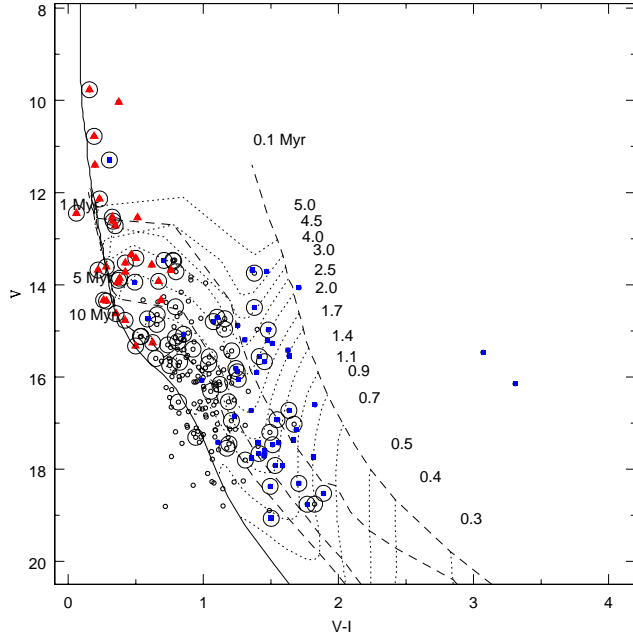


**Figure 10.**  $V/(V-I)$  CMD for variable stars in the region of the cluster NGC 281. The filled squares represent probable PMS variable stars, whereas triangles show MS stars. The variable stars belong to the field population is shown by open circles. The encircled points here refer to those stars which are having membership probability  $\geq 50\%$ . The continuous curve shows ZAMS by Girardi et al. (2002) while dashed lines represent PMS isochrones for 0.1, 1, 5, 10 Myrs (Siess et al. 2000). The PMS evolutionary tracks for different masses taken from Siess et al. (2000) are shown by dotted curves.

probability. The membership probability of variable stars along with proper motion values is given in Table 2. Fig. 11 shows the vector point diagram (VPD) of the proper motions for stars of the NGC 281. The highest concentrated area in the VPD gives 44 of 81 members identified from TCDs and CMD, and these 44 stars could be the most probable members of cluster. The 44 members distributed in the highest concentrated area in Fig. 11 have membership probabilities  $\geq 50\%$ . Out of 81 members, 37 stars with membership probabilities  $< 50\%$  could be considered as the least probable members of the cluster because of their locations in  $V/V-I$  CMD and  $J-H/H-K$  TCD. There are 35 field stars with membership probabilities  $\geq 50\%$ . Though the membership probabilities of all these 35 stars are  $\geq 50\%$  and 33 of which are located where PMS stars are found to be lying in  $V/V-I$  CMD, they could not be considered as members of the cluster because of their locations in  $J-H/H-K$  TCD.

#### 4 NATURE OF VARIABLE STARS

Of 228 periodic variables detected in the present work, 81 (30 MS and 51 PMS) stars are found to be associated with the cluster. The MS variable stars are classified according to their periods of variability, shape of light curves, as well as their locations in the Hertzsprung - Russell (HR) diagram. The  $H-R$  diagram for MS variables is shown in Fig. 12. The

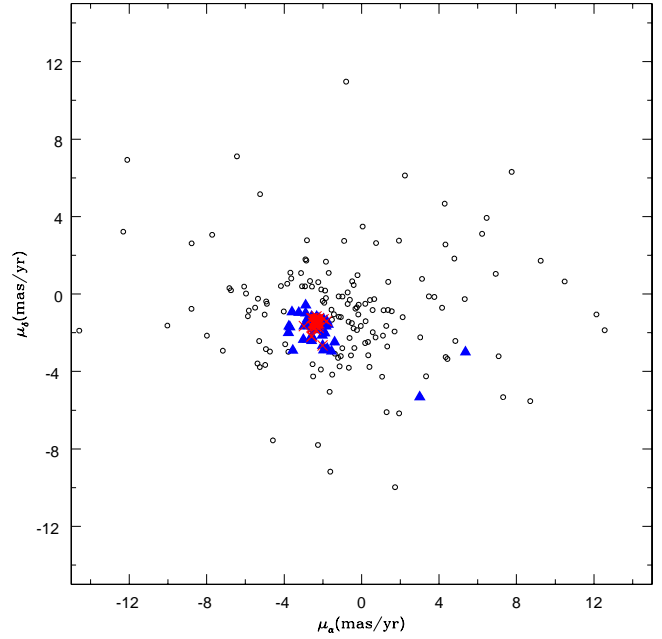


**Figure 11.** The VPD of the proper motions for stars in the NGC 281 region. Open circles represent proper motions of 223 stars (cf. section 3.4) while triangles represent variables with membership probabilities  $\geq 50\%$ . The crosses show present cluster members (both MS and PMS) with membership probabilities  $\geq 50\%$ .

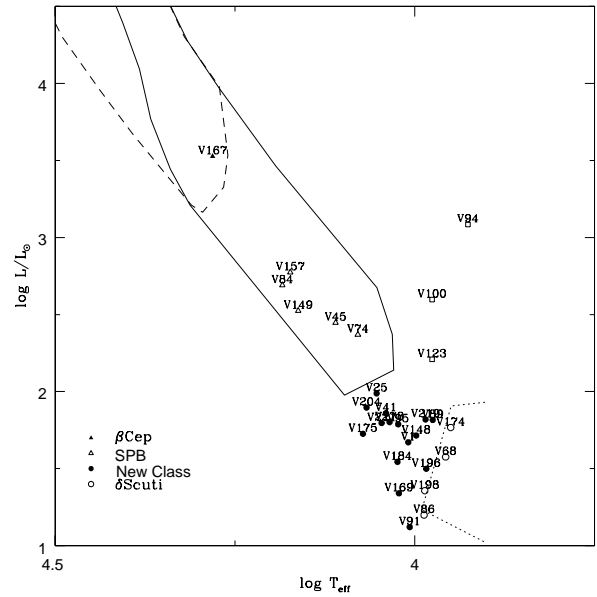


**Figure 12.**  $\log(L/L_{\odot})/\log T_{\text{eff}}$  diagram for the probable MS variable stars identified in the present study. The continuous curve represents the instability strip of SPB stars where as dotted curves shows the instability region of  $\delta$  Scuti stars. The dashed curve shows the location of  $\beta$  Cep stars (cf. Balona et al. 2011).

**Table 2.** The *VI* data, amplitude and period of variables in the open cluster NGC 281. The Proper motion data were taken from Gaia (Gaia Collaboration et al. 2018). The column Prob. refers to the membership probabilities of variable stars calculated using proper motion data.

ID	RA(2000)	Dec(2000)	<i>V</i> (mag)	<i>I</i> (mag)	$\mu_{RA}$ mas/yr	$\mu_{Dec}$ mas/yr	Prob.	Amplitude (mag)	Period (days)	Class.
V1	13.394370	56.588220	13.961±0.018	12.944±0.021	-5.497	-0.706	0.22	0.032	0.297	MS
V2	13.340740	56.511100	15.530±0.024	14.349±0.013	4.332	2.558	0.	0.045	0.375, 0.407	Field
V3	13.418240	56.627450	15.534±0.020	14.650±0.021	-5.376	-3.587	0.31	0.037	0.222,0.212	Field
V4	13.362610	56.548570	18.254±0.051	16.958±0.018	-0.24	-1.861	0.23	0.076	0.331,0.327	Field
V5	13.349920	56.541820	16.535±0.026	15.442±0.008	-4.89	-0.504	0.28	0.045	0.495	Field
V6	13.455430	56.695880	15.845±0.023	14.694±0.009	-0.207	0.974	0.08	0.103	0.157	Field
V7	13.405920	56.625330	16.091±0.018	15.137±0.011	-1.135	-3.733	0.34	0.035	0.572	Field
V8	13.408430	56.634080	16.162±0.018	15.040±0.011	-2.889	-0.987	0.62	0.045	0.573	Field
V9	13.413880	56.642560	17.391±0.037	-	-1.556	-0.809	0.36	0.052	0.351	Field
V10	13.400810	56.624510	16.165±0.020	15.073±0.014	1.293	-6.098	0.	0.040	0.583,0.441	Field
V11	13.385840	56.604010	15.376±0.021	14.236±0.017	1.73	-9.976	0.	0.043	0.754,0.412	Field
V12	13.349280	56.555970	17.728±0.029	15.912±0.398	7.309	-5.325	0.	0.072	0.811	PMS
V13	13.317420	56.511180	12.224±0.019	-	-1.888	-2.018	0.63	0.044	0.579,0.634,0.614	Field
V14	13.423000	56.666444	14.371±0.008	13.707±0.010	0.576	-1.972	0.17	0.046	0.488,0.522	Field
V15	13.419056	56.661000	18.807±0.242	18.088±0.065	3.759	-0.154	0.	0.261	0.129	Field
V16	13.397806	56.630806	15.236±0.008	14.425±0.008	-1.985	-1.454	0.61	0.039	0.492,0.499,0.441,0.434	Field
V17	13.375028	56.598694	15.991±0.010	15.223±0.012	2.121	-1.196	0.	0.052	0.628	Field
V18	13.388667	56.620694	15.668±0.011	14.215±0.009	-2.199	-1.252	0.61	0.068	0.751	PMS
V19	13.334667	56.553167	16.538±0.041	15.352±0.010	-1.781	-2.825	0.56	0.037	0.448	Field
V20	13.401583	56.653056	14.328±0.006	13.774±0.008	-0.659	-3.806	0.28	0.038	0.454,0.427	Field
V21	13.413111	56.674639	17.765±0.032	16.409±0.014	0.749	2.632	0.	0.075	0.334,0.331	PMS
V22	13.321028	56.541028	16.825±0.025	15.807±0.013	0.191	-0.505	0.16	0.049	0.487,0.530	Field
V23	13.315000	56.536750	14.161±0.006	13.325±0.009	-5.242	5.157	0.	0.020	0.530	Field
V24	13.394694	56.653278	17.153±0.021	16.062±0.011	-0.409	0.468	0.12	0.069	0.447	Field
V25	13.329500	56.559972	13.526±0.005	13.103±0.006	-2.191	-1.506	0.64	0.028	0.468	MS
V26	13.322417	56.552472	15.908±0.013	14.796±0.009	1.105	-2.151	0.1	0.035	0.750,0.816	Field
V27	13.332667	56.567500	14.648±0.007	13.990±0.007	-2.273	-1.534	0.65	0.037	0.308	Field
V28	13.362556	56.616000	15.407±0.010	14.550±0.012	1.378	0.626	0.	0.059	0.527	Field
V29	13.388639	56.654694	17.928±0.039	16.342±0.031	-	-	-	0.160	0.485,0.527	PMS
V30	13.324583	56.565278	17.918±0.066	16.386±0.013	-2.016	-2.658	0.61	0.078	0.306	PMS
V31	13.347389	56.599528	15.858±0.023	14.865±0.008	9.249	1.719	0.	0.059	0.481,901	Field
V32	13.410944	56.693083	18.270±0.045	17.206±0.025	-2.821	2.777	0.	0.127	0.481	Field
V33	13.390361	56.66475	16.673±0.017	15.657±0.012	0.184	-2.532	0.21	0.051	0.497,0.482	Field
V34	13.336667	56.587139	13.894±0.009	12.986±0.006	3.333	-4.249	0.45	0.058	0.654	Field
V35	13.323556	56.568694	16.602±0.017	14.775±0.011	-3.674	1.102	0.22	0.044	0.449	PMS
V36	13.375361	56.644583	17.438±0.062	16.596±0.032	-4.941	-2.843	0.42	0.201	0.788,0.447,0.737	Field
V37	13.299611	56.537639	14.727±0.007	13.745±0.008	-	-	-	0.035	0.354,0.386	Field
V38	13.354639	56.618389	17.470±0.033	15.956±0.012	-2.243	-1.486	0.65	0.087	0.722,0.779	PMS
V39	13.324583	56.580528	17.144±0.034	15.457±0.008	-1.381	-3.081	0.45	0.058	0.429,0.732,0.418	PMS
V40	13.347361	56.617222	15.168±0.017	14.335±0.007	-5.007	-1.064	0.28	0.076	0.489	Field
V41	13.289889	56.535167	13.682±0.008	12.922±0.006	0.33	-2.475	0.19	0.042	0.572	MS
V42	13.326389	56.590611	16.111±0.029	15.167±0.013	-5.968	0.027	0.28	0.066	0.735	Field
V43	13.385611	56.679278	17.504±0.051	16.099±0.017	-1.615	-9.175	0.	0.041	0.321	Field
V44	13.356528	56.638389	14.966±0.007	13.567±0.006	-1.843	-0.211	0.28	0.054	0.441,0.504	MS
V45	13.385694	56.683417	12.448±0.008	12.387±0.012	-2.225	-1.607	0.66	0.053	0.467	Field
V46	13.336500	56.612444	13.829±0.013	12.921±0.009	0.057	3.486	0.	0.082	0.489	Field
V47	13.278389	56.529556	13.746±0.012	12.368±0.009	-3.757	-1.657	0.56	0.049	0.347	Field
V48	13.275667	56.527500	17.048±0.044	15.738±0.011	0.207	-1.404	0.18	0.069	0.482,0.492	Field
V49	13.388472	56.694111	16.072±0.011	15.083±0.009	-8.785	-0.763	0.	0.068	0.475,0.507	PMS
V50	13.329250	56.608333	14.804±0.008	13.892±0.006	2.239	6.123	0.	0.035	0.412,0.423,0.318,0.245	Field
V51	13.346583	56.635944	16.205±0.013	15.203±0.008	1.93	2.755	0.	0.067	1.035	Field
V52	13.375139	56.677611	18.425±0.060	17.280±0.049	-2.084	0.236	0.21	0.105	0.456	Field
V53	13.276667	56.535389	18.757±0.074	16.933±0.023	-2.579	-1.517	0.68	0.140	0.468	Field
V54	13.323639	56.605444	17.450±0.092	16.260±0.011	-3.697	-1.71	0.57	0.105	0.476,0.864,0.516	Field
V55	13.367833	56.672722	18.308±0.053	16.601±0.013	-2.273	-1.315	0.62	0.296	0.511,1.02	PMS
V56	13.321417	56.610500	17.201±0.020	15.708±0.013	-2.175	-1.382	0.62	0.104	0.719,0.475	Field
V57	13.371333	56.686944	17.023±0.027	15.351±0.029	-1.723	-1.578	0.57	0.058	0.601,0.648	Field
V58	13.369972	56.685972	15.419±0.009	13.792±0.009	-0.149	-0.552	0.15	0.042	0.482,0.497,0.533	PMS
V59	13.297333	56.580694	17.802±0.037	16.491±0.012	-2.581	-1.163	0.64	0.069	0.423,0.449,0.433,0.482	Field
V60	13.298278	56.583806	16.130±0.017	15.044±0.006	12.129	-1.055	0.	0.056	0.468,0.684	Field
V61	13.362944	56.679222	15.964±0.014	15.119±0.016	-1.076	-3.21	0.4	0.062	0.828,0.451	Field
V62	13.280194	56.561361	13.715±0.014	12.917±0.008	-3.004	-2.357	0.66	0.017	0.325,0.251	Field
V63	13.282667	56.565722	17.248±0.024	16.248±0.016	-2.503	-4.255	0.34	0.069	0.499,0.532	Field
V64	13.285611	56.572167	15.434±0.011	14.224±0.006	-2.231	-1.469	0.64	0.061	0.336	Field
V65	13.288722	56.580389	16.583±0.024	15.651±0.009	-1.841	1.671	0.2	0.056	0.432,0.336,0.429,0.499	Field
V66	13.301639	56.599722	17.546±0.037	16.372±0.023	-2.03	-2.126	0.64	0.097	0.516,0.864,0.489,0.828	Field
V67	13.358639	56.683389	16.750±0.018	15.860±0.011	-0.986	-0.131	0.15	0.044	0.828,0.935,0.481,1.22	Field
V68	13.271528	56.556500	13.949±0.007	13.584±0.006	0.345	-3.165	0.23	0.043	0.217,0.336	MS
V69	13.264167	56.547889	14.910±0.007	14.127±0.007	0.572	-0.828	0.17	0.023	0.271	Field
V70	13.361861	56.690722	17.783±0.04	16.716±0.017	-0.411	-1.775	0.25	0.104	0.533,0.919	Field
V71	13.284639	56.582861	15.994±0.010	15.173±0.012	-3.836	0.531	0.28	0.047	0.467,0.794	Field
V72	13.361444	56.704306	15.658±0.009	14.968±0.009	-0.673	-1.428	0.27	0.042	0.459,0.481	Field
V73	13.276639	56.581278	15.198±0.007	14.346±0.006	1.137	-0.837	0.14	0.058	0.469	Field
V74	13.318472	56.642528	12.717±0.008	12.369±0.007	-2.254	-1.44	0.64	0.011	0.273,0.239,0.233	MS
V75	13.346361	56.683611	16.608±0.023	15.530±0.010	4.791	1.832	0.	0.073	0.171,0.302,0.498,0.460	Field
V76	13.236028	56.526250	17.417±0.025	16.308±0.013	-2.855	1.73	0.22	0.129	0.769	Field
V77	13.330972	56.665333	14.478±0.012	13.684±0.009	-1.839	-1.668	0.6	0.013	0.308,0.318	PMS
V78	13.359389	56.709222	14.062±0.008	12.353±0.011	-2.237	0.61	0.17	0.035	0.314,0.710,0.332,0.512	PMS
V79	13.269944	56.580111	17.225±0.040	16.297±0.017	-2.532	-3.626	0.44	0.055	0.459,0.471	Field
V80	13.254417	56.560833	13.464±0.007	12.676±0.011	-2.663	0.669	0.22	0.019	0.325	Field
V81	13.280000	56.604917	15.397±0.021	14.473±0.007	-1.558	-2.961	0.5	0.037	0.338	Field
V82	13.304917	56.643000	15.239±0.007	14.307±0.006	-1.515	-4.161	0.31	0.017	0.249,0.332	Field
V83	13.351472	56.712806	17.087±0.024	16.205±0.013	-3.783	-2.982	0.44	0.075	0.475	Field
V84	13.302139	56.643861	12.534±0.005	12.208±0.006	-2.579	-2.209	0.68	0.072	0.434	MS
V85	13.276806	56.608778	16.946±0.020	15.738±0.011	-3.248	-0.959	0.6	0.060	0.471,0.523	Field
V86	13.278083	56.612972	15.255±0.008	14.630±0.008	-2.451	-1.532	0.67	0.021	0.234,0.305,0.302	MS
V87	13.314944	56.671000	17.611±0.026	16.157±0.019	-0.72	-0.515	0.16	0.088	0.560	PMS
V88	13.336028	56.702222	18.896±0.127	17.407±0.031	-	-	-	0.238	0.332	Field
V89	13.236778	56.559639	13.344±0.007	12.876±0.007	-1.069	-1.191	0.32	0.017	0.328,0.332,0.343,0.498,0.348,7.745	MS
V90	13.323944	56.687389	17.106±0.023	16.158±0.012	-3.127	1.085	0.22	0.054	0.446	Field
V91	13.255417	56.588111	15.329±0.009	14.830±0.007	-2.382	-1.45	0.66	0.058	0.525	MS
V92	13.252111	56.584556								

Table 2. Continued.

ID	RA(2000)	Dec(2000)	V (mag)	I (mag)	$\mu_{RA}$ mas/yr	$\mu_{Dec}$ mas/yr	Prob.	Amplitude (mag)	Period (days)	Class.
V112	13.278083	56.670528	15.678±0.008	14.853±0.006	-2.807	-1.294	0.66	0.030	0.315	Field
V113	13.202000	56.564306	15.952±0.013	15.068±0.008	-2.919	0.396	0.28	0.096	14.399	Field
V114	13.226889	56.601361	18.373±0.050	16.878±0.029	-2.486	-1.704	0.68	0.132	0.572	PMS
V115	13.276500	56.675028	15.895±0.037	15.106±0.007	-3.946	-2.593	0.46	0.041	0.561	Field
V116	13.296611	56.704944	16.011±0.012	15.012±0.008	10.488	0.648	0.	0.064	1.068,0.489,0.525,1.147	Field
V117	13.307306	56.721611	15.929±0.019	14.887±0.010	-3.074	0.398	0.28	0.067	0.768	Field
V118	13.292306	56.701083	16.311±0.034	14.978±0.010	-1.699	1.091	0.13	0.046	0.524	Field
V119	13.181250	56.540222	15.303±0.021	14.566±0.007	-3.777	-1.995	0.55	0.018	0.211	Field
V120	13.237139	56.623556	17.417±0.045	16.015±0.018	-14.581	-1.891	0.	0.105	0.541,3.363,1.0649	PMS
V121	13.201694	56.571583	17.715±0.059	16.265±0.014	-7.989	-2.151	0.	0.111	0.747,1.248	PMS
V122	13.283194	56.691722	15.982±0.009	15.021±0.007	-10.029	-1.629	0.	0.036	0.455,1.286,0.533,1.177	Field
V123	13.226056	56.610611	12.545±0.016	12.032±0.004	-1.531	-1.328	0.49	0.049	0.760	MS
V124	13.287778	56.700750	18.525±0.110	16.635±0.047	-1.797	-1.401	0.56	0.392	4.0414	PMS
V125	13.203333	56.579972	18.760±0.078	16.991±0.019	-2.396	-1.546	0.67	0.188	0.543	PMS
V126	13.259917	56.670000	14.740±0.008	14.153±0.006	-2.339	-1.386	0.64	0.015	0.061,0.531	PMS
V127	13.216833	56.609694	15.803±0.009	14.787±0.007	0.722	-2.241	0.16	0.045	0.521,0.504	Field
V128	13.240056	56.644250	15.557±0.006	14.143±0.005	-2.343	-1.431	0.65	0.017	0.251,0.253,0.249	PMS
V129	13.187167	56.570806	14.260±0.008	13.553±0.005	-5.351	-0.243	0.25	0.012	0.237	Field
V130	13.173333	56.550944	15.188±0.006	14.330±0.006	-12.102	6.927	0.	0.017	0.290	Field
V131	13.203030	56.595610	18.480±0.074	-	-3.555	-2.904	0.5	0.181	0.453,0.883,0.447	Field
V132	13.205056	56.603056	17.725±0.039	16.961±0.041	-2.01	-0.357	0.35	0.155	0.516,0.533	Field
V133	13.212694	56.615806	13.472±0.009	12.763±0.006	-2.329	-1.424	0.65	0.040	0.356,0.571	PMS
V134	13.252194	56.676028	17.145±0.020	16.058±0.017	4.846	-2.423	0.35	0.041	0.322	Field
V135	13.214750	56.624694	14.859±0.017	14.203±0.022	-2.317	-1.364	0.64	0.051	0.541	Field
V136	13.248972	56.674944	16.654±0.027	15.891±0.012	-4.976	-3.663	0.28	0.034	0.433	Field
V137	13.232778	56.656556	15.072±0.007	14.218±0.006	-2.326	-1.451	0.65	0.032	0.479,0.545,1.326	PMS
V138	13.228500	56.650861	15.544±0.015	13.909±0.007	-0.721	0.083	0.13	0.026	0.615,0.686	PMS
V139	13.214556	56.630917	14.734±0.020	13.575±0.014	-2.306	-1.538	0.66	0.021	0.287	Field
V140	13.217222	56.639472	16.544±0.015	15.728±0.011	-2.886	-0.572	0.53	0.040	0.658, 0.631	Field
V141	13.167694	56.569250	14.380±0.007	13.656±0.007	-4.166	0.413	0.28	0.013	0.339	Field
V142	13.242861	56.679806	14.690±0.009	13.884±0.008	-5.255	-3.775	0.26	0.022	0.427,0.485	Field
V143	13.203639	56.625417	9.769±0.025	9.612±0.014	-2.366	-1.437	0.66	0.059	0.575	MS
V144	13.243528	56.686000	13.687±0.008	12.326±0.009	1.061	-4.27	0.31	0.022	0.443,0.554,0.423	PMS
V145	13.207417	56.635583	13.609±0.036	13.327±0.009	-2.347	-1.495	0.66	0.027	0.530,1.22	MS
V146	13.161417	56.569083	15.752±0.013	14.937±0.008	-7.714	3.06	0.	0.015	0.364	Field
V147	13.155250	56.560139	17.427±0.028	15.868±0.015	4.293	4.668	0.	0.137	3.302,4.474	PMS
V148	13.185333	56.607833	13.904±0.014	13.532±0.006	-2.432	-1.601	0.67	0.039	0.469,0.332	MS
V149	13.201139	56.631694	12.816±0.014	12.286±0.012	-2.37	-1.479	0.66	0.023	0.554,0.539	MS
V150	13.189917	56.620972	14.799±0.007	13.725±0.007	-2.279	-1.494	0.65	0.029	0.334,0.490,0.460	PMS
V151	13.201778	56.640028	15.887±0.011	14.636±0.007	-2.404	-1.552	0.67	0.050	1.095,1.23	PMS
V152	13.184611	56.618056	11.293±0.010	10.988±0.004	-2.371	-1.282	0.64	0.016	0.460,0.342	PMS
V153	13.168778	56.597500	13.467±0.007	12.692±0.005	-2.314	-1.58	0.66	0.018	0.111	Field
V154	13.188833	56.628194	14.703±0.008	13.601±0.007	-2.404	-1.446	0.66	0.060	0.550,0.513,1.094	PMS
V155	13.202389	56.648917	16.273±0.015	15.507±0.014	-5.289	-2.426	0.42	0.084	0.710	Field
V156	13.189528	56.631917	13.943±0.011	13.450±0.007	-2.36	-1.417	0.66	0.041	0.946,0.492	PMS
V157	13.180361	56.620000	12.137±0.012	11.905±0.005	-2.484	-1.503	0.67	0.034	0.540,0.520	MS
V158	13.191611	56.639417	15.208±0.021	13.733±0.006	-4.019	-0.898	0.47	0.027	0.526	PMS
V159	13.152389	56.583083	15.358±0.016	14.599±0.007	-6.066	0.384	0.28	0.083	4.22	Field
V160	13.153639	56.587778	16.498±0.021	15.270±0.010	0.406	-3.766	0.26	0.163	0.635,3.15,1.99,1.42	Field
V161	13.191528	56.648278	14.613±0.006	13.785±0.006	8.711	-5.531	0.	0.018	0.520,0.538	Field
V162	13.132417	56.564167	17.129±0.021	15.933±0.012	-4.581	-7.56	0.	0.127	0.475	Field
V163	13.158000	56.601944	16.311±0.012	15.256±0.008	-2.505	-1.543	0.67	0.065	0.830	Field
V164	13.188667	56.650472	19.067±0.260	17.564±0.035	-2.326	-1.157	0.61	0.182	0.463	PMS
V165	13.185139	56.646028	15.815±0.011	14.574±0.007	-2.283	-1.374	0.64	0.105	0.618,0.593,0.657,0.630	PMS
V166	13.192500	56.658194	14.881±0.008	13.625±0.005	0.653	-0.263	0.16	0.019	0.682,0.651	PMS
V167	13.151000	56.600222	10.779±0.008	10.587±0.012	-2.595	-1.254	0.65	0.023	0.251,0.247	MS
V168	13.151556	56.609667	15.144±0.009	14.350±0.006	-2.43	-1.371	0.65	0.018	0.1045	Field
V169	13.139250	56.594083	14.769±0.009	14.349±0.006	-2.261	-1.328	0.63	0.015	0.429,0.411,0.442,0.294	MS
V170	13.161556	56.627167	14.353±0.009	13.463±0.006	4.432	-3.352	0.37	0.032	0.699	Field
V171	13.163139	56.630444	16.049±0.010	14.790±0.008	-2.214	-1.744	0.67	0.098	0.514,1.27	PMS
V172	13.169556	56.645500	15.751±0.011	15.000±0.010	-1.96	-2.901	0.56	0.023	0.639	Field
V173	13.111889	56.561833	17.021±0.028	15.916±0.009	7.079	-3.215	0.	0.098	0.459	Field
V174	13.139000	56.604528	13.425±0.012	12.924±0.006	-2.223	-1.303	0.62	0.020	0.235,0.207,0.423	MS
V175	13.220806	56.727778	14.337±0.011	13.651±0.009	-0.317	-0.755	0.16	0.032	0.397,0.469	MS
V176	13.161389	56.642556	15.668±0.010	14.739±0.006	-5.872	-1.146	0.19	0.026	0.625	Field
V177	13.182528	56.674722	17.048±0.023	16.169±0.013	1.277	-1.646	0.09	0.032	0.545,0.403	Field
V178	13.174222	56.666472	13.679±0.014	13.458±0.005	-2.307	-1.299	0.63	0.026	0.644,0.658,0.416	MS
V179	13.135278	56.609444	15.120±0.009	14.580±0.007	-2.878	-1.569	0.68	0.056	0.503,1.096	Field
V180	13.213250	56.729417	17.177±0.024	16.217±0.015	0.435	-0.315	0.16	0.021	0.481,0.435	Field
V181	13.190917	56.700778	16.013±0.017	14.820±0.007	4.343	-3.254	0.34	0.054	0.450	Field
V182	13.146306	56.643361	16.133±0.010	14.923±0.015	-2.9	1.791	0.22	0.033	0.435,0.751	Field
V183	13.130361	56.620167	17.300±0.052	16.214±0.012	-2.254	-7.795	0.	0.055	0.660	Field
V184	13.144639	56.659694	14.354±0.008	14.070±0.006	-2.384	-1.322	0.65	0.027	0.752	MS
V185	13.112861	56.615694	17.578±0.027	16.465±0.019	-0.039	-1.647	0.2	0.092	0.474	PMS
V186	13.125889	56.635694	15.591±0.011	14.844±0.007	-0.503	-1.505	0.24	0.030	0.447	Field
V187	13.193556	56.738056	14.492±0.008	13.114±0.010	-2.364	-1.663	0.68	0.048	0.510,0.477	Field
V188	13.094694	56.597611	16.724±0.016	15.090±0.008	-1.962	-1.299	0.57	0.125	3.591	PMS
V189	13.120167	56.636556	17.298±0.048	16.315±0.025	1.362	-0.823	0.1	0.062	0.606	Field
V190	13.167889	56.707472	18.349±0.070	17.424±0.034	-2.563	0.383	0.24	0.117	0.515	Field
V191	13.069278	56.707472	15.046±0.009	14.159±0.009	1.704	-1.934	0.	0.064	0.456	Field
V192	13.168028	56.713917	17.189±0.026	16.395±0.016	-4.925	-0.384	0.28	0.058	0.499,0.245	Field
V193	13.116028	56.639722	15.598±0.010	14.950±0.009	-2.385	-1.477	0.66	0.044	0.471,0.447,0.491,0.454	Field
V194	13.086056	56.597417	16.107±0.026	15.176±0.023	1.325	-2.71	0.	0.059	0.539,0.530	Field
V195	13.175667	56.730944	13.483±0.006	12.703±0.010	5.368	-2.997	0.5	0.034	0.976	Field
V196	13.141917	56.687722	14.331±0.007	14.069±0.007	-2.527	-1.242	0.65	0.036	0.487	MS
V197	13.091861	56.614639	16.785±0.030	15.965±0.012	-6.828	0.302	0.43	0.047	0.454	Field
V198	13.108000	56.641861	14.624±0.009	14.270±0.007	-2.436	-1.789	0.68	0.047	0.255,0.318,0.340	MS
V199	13.152778	56.711944	18.092±0.115	17.060±0.023	-3.634	0.803	0.26	0.071	0.536,0.488	Field
V200	13.132500	56.688556	15.192±0.010	13.885±0.007	-1.174	-1.174	0.37	0.037	0.492,0.460,0.530	PMS
V201	13.159194	56.734167	16.063±0.012	15.240±0.011	1.94	-6.164	0.	0.050	0.527,0.758,0.478	Field
V202	13.163278	56.740722	16.229±0.042	15.504±0.010	-4.733	-2.97	0.4	0.		

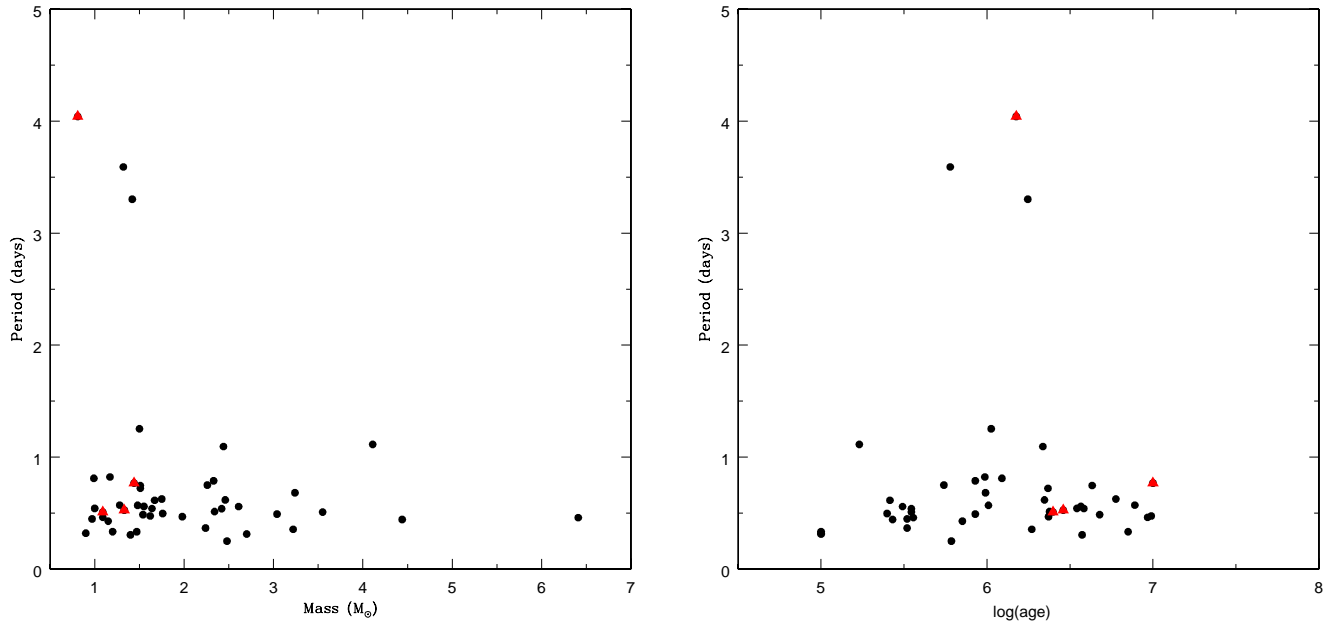


**Figure 13.** Rotation period of TT variables as a function of mass and age. Filled circles represent WTTs while triangle shows CTTSs.

location of variable stars in the  $H-R$  diagram has been estimated with the help of their intrinsic colour index  $(B-V)_0$  and  $V$  magnitudes. The  $U$ ,  $B$ , and  $V$  magnitudes are available for 29 MS periodic variables. The  $U$  data of V145 is not available. The intrinsic colour  $(B-V)_0$  of variable stars has been estimated using the Q-method (Gutiérrez-Moreno 1975). For determination of luminosity and temperature we require  $V$  magnitudes, distance of the cluster and relations provided by Torres (2010). The details of the procedure for obtaining luminosity and temperature of the star can be found in Lata et al. (2019). We have plotted  $(L/L_\odot)$  versus temperature diagram for 29 MS variables in Fig. 12. Thus, based on location of variables in the  $H-R$  diagram we have identified one variable as  $\beta$  Cep candidate. The  $\beta$  Cep stars are massive stars which are found to be located near the MS in the  $H-R$  diagram. Their spectral types range from O to B. These variables pulsate with short periods. Multiple periods are often found in these stars (Jager et al. 1982). Star V167 is detected as  $\beta$  Cep candidate with a period about 0.2 days in the present work. Five slowly pulsating B-type (SPB) candidates were also identified in the present work. SPB stars as their name suggests, are B spectral type stars. Their typical periods are in the range from 0.5 to 5 days and sometimes they show multiperiodicity. Waelkens (1991) studied SPB stars and named these early-type variables as ‘SPB stars’. The characteristics (periods and shape of light curves) of present variables detected as SPB stars are consistent with the class. The present sample of MS variables also consists of 15 new class variables among MS variable members. The new class variable stars have properties similar to the ones discovered in NGC 3766 by Mowlavi et al. (2013). The periods and amplitudes of new class variable stars detected by Mowlavi et al. (2013) range from 0.1 to 0.7 days and 1 to 4 mmag, respectively. The present new class variable stars have periods between 0.25 to 0.80 days.

Additionally, we have also detected 4 stars which could be  $\delta$  Scuti type variables. Their periods are found to be in the range of  $\sim 0.22 - 0.25$  days. These  $\delta$  Scuti stars are found to be pulsators which are located on/near the MS in the classical cepheid instability strip. These stars pulsate with period upto 5 or 6 hours. Three stars V94, V100 and V123 are neither lying on any instability regions of  $H-R$  diagram nor in the location of new class variable. These stars might be field stars or belong to the PMS population.

In the present study we have detected 51 PMS stars. In general, the PMS objects are classified as T Tauri stars (TTSs) and Herbig Ae/Be stars. The TTSs are very young low mass stars (mass  $\lesssim 3M_\odot$ ) which are still contracting and moving towards the MS (Herbig 1957, 1977), whereas PMS stars of intermediate mass ( $\gtrsim 3-10M_\odot$ ) with emission lines are considered as Herbig Ae/Be stars (Herbig 1960; Strom et al. 1972; Finkenzeller & Mundt 1984). The TTSs are further classified as Weak line TTSs (WTTs) and Classical TTSs (CTTSs) on the basis of the strength of the  $H\alpha$  emission line (Strom et al. 1989) which is measured by its equivalent width (EW). The WTTs show weak  $H\alpha$  ( $EW \leq 10\text{\AA}$ ) emission with almost negligible infrared excess, whereas CTTSs generally have a strong  $H\alpha$  emission line with  $EW > 10\text{\AA}$ , large ultraviolet and infrared excesses. Both CTTSs and WTTs show strong variability across all wavelengths and their brightness varies from a few minutes to years (see e.g., Appenzeller & Mundt 1989). The brightness variation of TTSs are thought to occur most probably due to the presence of cool and/or hot spots on their surface (Herbst et al. 1987, 1994), which may originate due to several mechanisms such as circumstellar disk material, accretion and magnetic field (Herbst et al. 1994).

The cool spots on the surface of the stars are produced due to stellar magnetic fields on the photosphere and rotate with the star. If these spots are symmetrically distributed

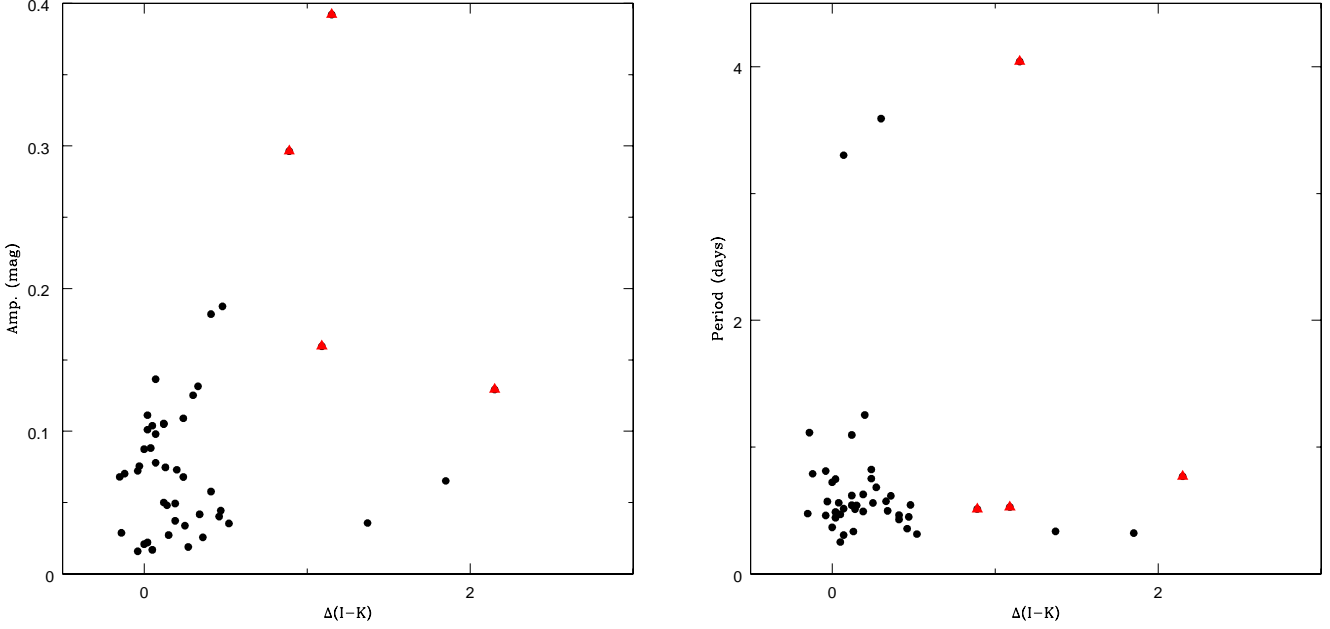


**Figure 14.** Amplitude and rotation period of TT variables versus  $\Delta(I - K)$ . The symbols are same as in Fig. 13.

over the photosphere, periodic brightness variations are observed in the light curves of the stars. The cool spots on the photosphere of stars are responsible for brightness variation in WTTs and these objects are found to be fast rotators as they have either thin or no circumstellar disk. WTTs are characterized by smaller stellar flux variations (a few times 0.1 mag).

Accreting CTTs, surrounded by circumstellar disks and have hot spots on the surface produced by accreting material from disks on to the stars, show a complex behaviour in their optical and NIR light curves (Scholz et al. 2009). Irregular or non-periodic variations are produced because of changes in the accretion rate. The time-scales of brightness variation range from hours to years. Although the hot spots cover a smaller area on the stellar surface, their higher temperature produces larger variability amplitude (Carpenter, Hillenbrand & Skrutskie 2001). The Herbig Ae/Be stars also show variability as they cross the instability strip in the HR diagram on their way to the MS. However, exact cause of variability in Herbig Ae/Be is still not known.

Of 51 probable PMS stars identified in the present work, 42, 4 and 5 are classified as WTTs, CTTs and Herbig Ae/Be stars, respectively. The amplitudes of WTTs ranges from  $\sim 0.015$  mag to  $\sim 0.19$  mag, while periods of most WTTs are found in the range of  $\sim 0.25$  to  $\sim 1.12$  days. The periods and amplitudes of CTTs are found to vary  $\sim 0.48$  to  $\sim 4$  days and  $\sim 0.13$  to  $\sim 0.39$  mag, respectively. The above results suggest that stars with disk i.e., CTTs have relatively larger amplitudes than the WTTs and indicate that variability in CTTs could be due to the presence of hot spot on the stellar surface (see e.g., Carpenter, Hillenbrand & Skrutskie 2001, Grankin et al. 2007, 2008, Lata et al. 2019). Similar results have been found in our earlier studies (Lata et al. 2019, 2016; Sinha et al. 2020).

Since the present sample of PMS stars is dominated

by WTTs (43 stars), we will further focus our analysis to understand the evolution of rotation period and amplitude of WTTs identified in the present work. The masses and ages of PMS variables were estimated by comparing present observations with the theoretical models to study the evolution of amplitude and period of PMS stars. The procedure for estimation of mass and age is given in Lata et al. (2019) and Chauhan et al. (2009). For this, we have used PMS isochrones of Siess et al. (2000) in the age range of 0.1 to 10 Myr with an interval of 0.1 Myr and  $V/V - I$  CMD of the cluster. These theoretical isochrones corrected for the distance and reddening were compared with the locations of PMS stars in the  $V/V - I$  CMD. Finally, we determine the mass and age of the PMS star corresponding to the closest isochrone on the CMD. The dependence of rotation period of TTSs (i.e., WTTs and CTTs) on age and mass is shown in Fig. 13 which reveals that rotation period of WTTs does not depend either on age or mass of the stars. However, the slowest rotators in the present study are low mass ( $\sim 1M_{\odot}$ ) stars.

WTTs have either thin or no circumstellar disk, it will be useful to estimate the influence of circumstellar disks on period and amplitude of these variable stars. The studies available in the literature e.g., Herbst et al. (2000); Littlefair et al. (2005); Cieza & Baliber (2007); Cody et al. (2018), have used various disk indicators, such as EW of the  $H\alpha$  emission line and Ca II triplet lines,  $\Delta(H - K)$  and  $\Delta(I - K)$  excess, disk fraction, etc. In the present study we have used  $\Delta(I - K)$  excess which is defined as below (cf. Hillenbrand et al. 1998);

$$\Delta(I - K) = (I - K)_{obs} - (A_I - A_K) - (I - K)_0$$

where  $(I - K)_{obs}$ ,  $(I - K)_0$ ,  $A_I$  and  $A_K$  are the observed colour, intrinsic colour of the star, interstellar extinction in the  $I$  and  $K$  bands, respectively. The  $A_V$  value is taken as 0.99 mag as determined using the relation  $A_V/E(B - V)$ .

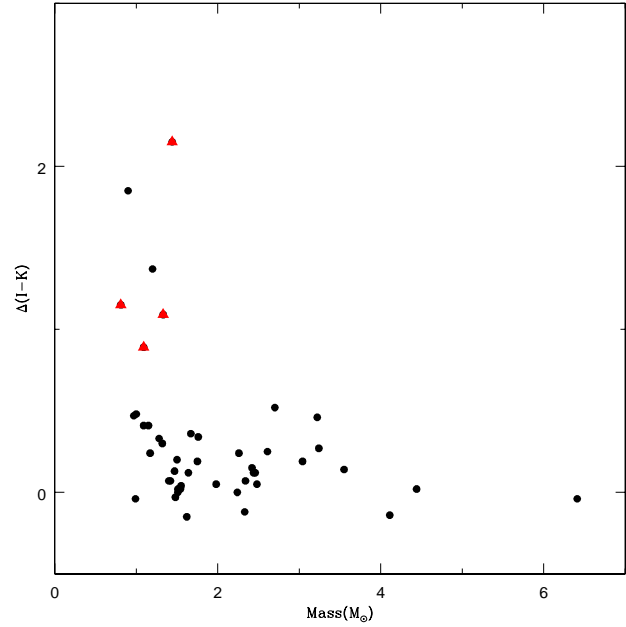


The values of  $A_I$  and  $A_K$  are estimated using the relations given by Cohen et al. (1981). To obtain intrinsic  $(I - K)_0$  of variables we have used PMS evolutionary models of Siess et al. (2000) of a given mass and age. Fig. 14 displays the amplitude and period of TT variables as a function of  $\Delta(I - K)$ . It is evident from Fig. 14 that the majority of WTTs have  $\Delta(I - K) < 0.3$  mag, hence they can be considered as disk-less sources. Apparently, no influence of  $\Delta(I - K)$  either on amplitude or rotation of WTTs is noticed. It is worthwhile to mention that a correlation between  $\Delta(I - K)$  and amplitude as well as period of CTTSs in the sense that larger values of the disk indicator, i.e.,  $\Delta(I - K)$  corresponds to relatively larger amplitude variations has been reported in previous studies (e.g., Dutta et al. 2018, Sinha et al. 2019). Similarly, larger values of  $\Delta(I - K)$  indicates longer rotation periods. An extensive study of ONC carried out by Herbst et al. (2000, 2002) reveals a strong correlation between rotation period and infrared excess, suggesting that the observed rotation period distribution could be due to the disk-locking mechanism. Similar results were reported by Edwards et al. (1993) and the physical interpretation proposed by the authors was that the disks slow the rotation of stars through magnetic interaction (Koenigl 1991; Ostriker & Shu 1995). An increasing trend in disk fraction with period in ONC and NGC 2264 was reported by Cieza & Baliber (2007). However, Littlefair et al. (2005) did not find any correlation between the  $H\alpha$  equivalent width or  $(K - L)$  excess and the rotation period of the stars.

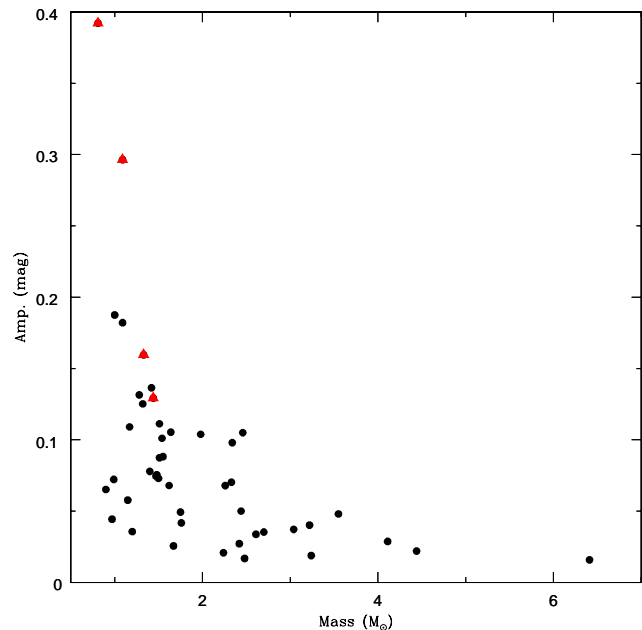
To check the dependence of  $\Delta(I - K)$  on the stellar mass, we plot these parameters for all the PMS variables identified in the present study in Fig. 15 which reveals that higher values of NIR excess are associated with relatively low mass stars. This is consistent with the result that the slowest rotators in the present study are low mass ( $\sim 1.0 M_\odot$ ) CTTSs (cf. Fig. 13).

Fig. 16 plots amplitude of variability as a function of mass of the PMS variables, which manifests that the amplitude decreases with the increase in mass.

Fig. 17 displays amplitude as a function of age. It is interesting to note that the amplitude of variability of WTTs show an increase for relatively older stars. An inspection of figure 20 by Sinha et al. (2019) also indicates that the youngest WTTs (age  $< 1$  Myr) in the Sh 2-170 H II region also show lower value of amplitudes as compared to older WTTs. In the inset of Fig. 17 we plot data for WTTs from our previous studies for the clusters Be 59, NGC 1893, NGC 7380 and Stock 8 (Lata et al. 2011, 2012, 2016 and 2019). The same trend has been noticed in previous data also. Grankin (1999, 2013) and Grankin et al. (2008) have shown that a small periodicity amplitude suggests a more uniform distribution of spots over the stellar surface, while a large amplitude is typical of the case where the spots are concentrated in one or two high-latitude regions, i.e., they are distributed highly non uniformly. These conclusions are also confirmed by the Doppler mapping of the surfaces of selected PMS stars (Grankin 2013). Thus, Fig. 17 seems to suggest that configuration/distribution of spots on the photosphere of WTTs changes as they become older. The smaller amplitude for relatively larger mass ( $\gtrsim 2.5 M_\odot$ ) as noticed in Fig. 16 could be either due to dispersal of disk or uniform distribution of spots over stellar surface. It has been reported in our earlier studies that the disk dispersal



**Figure 15.** Excess  $\Delta(I - K)$  as a function of mass for TT variables. The symbols are same as in Fig. 13.



**Figure 16.** Amplitude of present TT variable candidates as a function of mass. The symbols are same as in Fig. 13.

mechanism is less efficient for relatively low mass stars (Lata et al. 2011, 2012, 2016).

The present study consists of 147 variables which could belong to the field population in the direction of NGC 281. Based on their light curves and variability characteristics, these stars could be RR Lyrae,  $\delta$  Scuti, or binaries type vari-

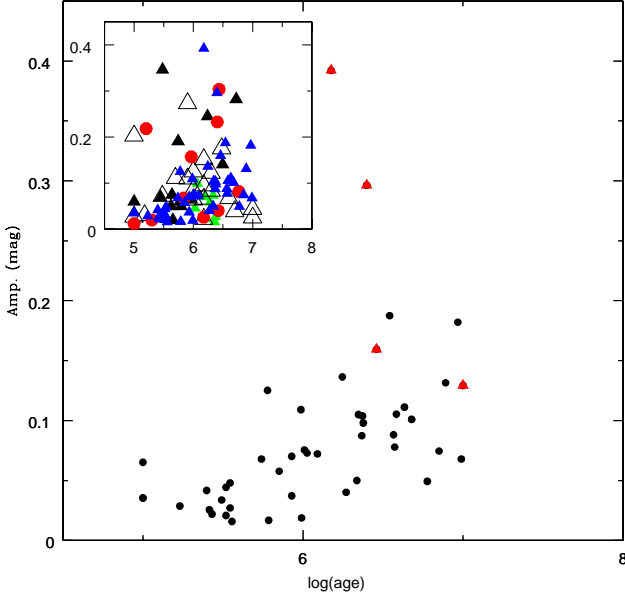


**Figure 17.** Amplitude of present TT variable candidates as a function of age. The symbols are same as in Fig. 13. Inset plots data for WTTs taken from our earlier works (Lata et al. 2011, 2014, 2016 and 2019).

ables. As present study contains a few interesting variable stars which need to be characterized individually.

Star numbered V6 has a period of 0.157 days and an amplitude of 0.103 mag which indicates that the star might be a  $\delta$  Scuti variable. The shape of the light curve also resembles the light curve of  $\delta$  Scuti variables having nearly sinusoidal nature.

Star V15 has  $V$  magnitude about 18.81 mag and it might belong to the field star population. With a period of 0.129 days and an amplitude of 0.261 mag, variable star V15 is suspected to be of the Ellipsoidal variables type which is a subgroup of the rotating variable stars. The light curve is W-shaped with minima portion substantially broader than the maxima (peak) which is quite sharp. The two clearly visible minimas might not be equally deep due to stronger limb-darkening effect on the pointed portion of the more elongated star.

Star V42 has a period of 0.735 days and an amplitude of 0.066 mag. It could possibly be RR Lyrae (RRab) type variable since it has a period which is similar to RRab type variables. In addition to this, it has asymmetric shaped light curve which is again a characteristic of RR Lyrae type variables.

Star V123 has a period of 0.76 days and amplitude of 0.049 mag. This star may be Cataclysmic variable of nova type as the light curve indicates that the amplitude decreases gradually as in case of cataclysmic variable.

Star V126 has a period of 0.06 days and 0.531 days with an amplitude of 0.015 mag. It is considered as PMS star (Herbig Ae/Be) in the present work. The shape of the light curve of this star indicates that this might be RS Canum Venaticorum eclipsing binary. In addition to this, amplitude

of such variables are in the range of 0.01 to 0.6 mag and the amplitude of this star also comes in this range.

In the present work star V152 is considered as a PMS star. Sharma et al. (2012) identified star V152 as a PMS source. However, this star in  $J - H/H - K$  TCD does not lie in the region of class I, class II, II or Herbig Ae/Be. In fact, this is a bright star of  $V$  magnitude around 11.3 mag, and in  $V/V - I$  CMD it is located on/near MS with other identified MS stars. It has a period of 0.46 days and amplitude of 0.016 mag, and its variability characteristics also reveals that it could be a slowly pulsating star.

The period of star V153 and V168 is 0.111 and 0.105 days, respectively and their amplitude is found as 0.018 mag. Based on variability characteristics, these stars could be of  $\delta$  Scuti type variables.

## 5 SUMMARY

The present work detected 228 periodic variables in the field where young open cluster NGC 281 is located. The association of variables to the cluster has been discussed on the basis of TCDs, CMD and kinematic data. The membership probabilities of 223 stars have been determined using Gaia proper motion data. Using the present time series photometric data we have detected a number of PMS, MS and field variable stars. Eighty one of 228 variables are members, with 30 MS members and 51 PMS members. Based on their periods and light curves shape, and locations in the  $H - R$  diagram we have characterized MS variable stars into different types of variability. These MS variables are classified as  $\beta$  Cep,  $\delta$  Scuti, SPB and new class type variables. The identified PMS variable stars are characterized as CTTs, WTTs and Herbig Ae/Be stars. The present study also indicates that the CTTs vary with larger amplitude in comparison to the WTTs. The masses and ages of PMS stars have been derived using CMD and PMS theoretical models. It is found that rotation period of WTTs does not depend either on age or mass of the stars. Amplitude and mass of TT variables are found to be correlated in the sense that relatively massive stars ( $\gtrsim 2.5M_{\odot}$ ) have smaller amplitudes. This could be due to lack of disk or uniform distribution of spots on the photosphere of the stars. We also note that the amplitude of variability of WTTs increases with age, suggesting that the configuration/distribution of spots on the surface of WTTs changes with their age. There are 147 variables which could belong to the field population. These field variables could be RR Lyrae,  $\delta$  Scuti, or binaries type variables.

## 6 ACKNOWLEDGMENT

We are thankful to the referee for careful reading of the paper and valuable suggestions/comments.

## AVAILABILITY OF DATA

The data underlying this article will be shared on reasonable request to the corresponding author.

The data underlying this article are available in 2MASS

(<https://vizier.u-strasbg.fr/viz-bin/VizieR?source=II/246>)  
and Gaia (<https://gea.esac.esa.int/archive/>).

## REFERENCES

- [ Appenzeller I., & Mundt R., 1989, *Astron. Astrophys. Rev.* 1, 291
- [ Arcos C., Kanaan S., Chavez J., Vanzi L., Araya I., Cure M., 2018, *MNRAS*, 474, 5287
- [ Balona L. A., Pigulski A., Cat P. De, Handler G., Gutiérrez-Soto J., Engelbrecht C. A., Frescura F., Briquet M., et al., 2011, *MNRAS*, 413, 2403
- [ Bessell M. S., Brett J. M., 1988, *PASP*, 100, 1134
- [ Burger M., de Jager C., van den Oord, G. H. J., Sato N., 1982, *A&A*, 107, 320
- [ Carpenter J. M., Hillenbrand L. A., Skrutskie M. F., 2001 *AJ*, 121, 3160
- [ Cabrera-Cano J. and Alfaro E. J., 1990, *A&A*, 235, 94
- [ Chauhan N., Pandey A. K., Ogura K. et al, 2009, *MNRAS*, 396, 964
- [ Cutri R. M. et al., 2003 , 2MASS All Sky Catalog of Point Sources, VizieR Online Data Catalog, University of Massachusetts and Infrared Processing and Analysis Center (IPAC/California Institute of Technology), 2246, 0 <https://vizier.u-strasbg.fr/viz-bin/VizieR?source=II/246>
- [ Cohen J. G., Persson S. E., Elias J. H., Frogel J. A., 1981, *ApJ*, 249, 481
- [ Cody A. M., Hillenbrand L. A. 2018, *AJ*, 156, 71
- [ Cieza Lucas, Baliber Nairn, 2007, *ApJ*, 671, 605
- [ Dutta S., Mondal S., Joshi S., Das R., 2019, *BSRSL*, 88, 103
- [ de Jager C., Sato, N., Burger M., Neven L., 1982, *Ap&SS*, 83, 411
- [ Edwards S., Strom S. E., Hartigan P., Strom K. M., Hillenbrand L. A., Herbst W., Attridge J., Merrill K. M., Probst R., Gatley I., 1993, *AJ*, 106, 372
- [ Elmegreen B. G. & Lada C. J., 1978, *ApJ*, 219, 467
- [ Finkenzeller U., Mundt R., 1984, *A&AS*, 55, 109
- [ Gaia Collaboration et al. 2018, *A&A*, 616, 13 <https://gea.esac.esa.int/archive/>
- [ Getman K. V., Feigelson E. D., Sicilia-Aguilar A., et al., 2012, *MNRAS*, 426, 2917
- [ Girardi L., Bertelli G., Bressan A., Chiosi C., Groenewegen M. A. T., Marigo P., Salasnich B., Weiss A., 2002, *A&A*, 391, 195
- [ Grankin K. N., Melnikov S. Yu., Bouvier J., Herbst W., Shevchenko V. S., 2007, *A&A*, 461, 183
- [ Grankin K. N., Bouvier J., Herbst W., Melnikov S. Y., 2008, *A&A*, 479, 827
- [ Grankin K. N., 2013, *Astronomy Letters*, 2013, Vol. 39, 446
- [ Grankin K. N., 1999, *Astron. Lett.* 25, 526
- [ Gutiérrez-Moreno A., 1975, *PASP* 87, 805
- [ Herbig G. H., 1960, *ApJS*, 4, 337
- [ Herbst W., Herbst D. K., Grossman E. J., Weinstein D., 1994, *AJ*, 108, 1906
- [ Herbst W., Booth J. F., Korett F. L., et al, 1987, *AJ*, 94, 13
- [ Herbst W., Bailer-Jones C. A. L., Mundt R., Meisenheimer K., Wackermann R., 2002, *A&A*, 396, 513
- [ Herbst W., Maley J. A., Williams E. C., 2000, *AJ*, 120, 349
- [ Ivers Carol B., Booker M., Piper M., Powers L., Ali B., Wolk S. J., 2014, *NITARP*, AAS, 22324419
- [ Jose J., Pandey A. K., Samal M. R., Ojha D. K., Ogura K., Kim J. S., Kobayashi N., Goyal A., Chauhan N., Eswaraiah C., 2013, *MNRAS*, 432, 3445
- [ Koenigl ArieH, 1991, *ApJ*, 370L, 39
- [ Landolt A. U., 1992, *AJ*, 104, 340
- [ Lata S., Pandey A. K., Maheswar G., Mondal S. and Kumar B., 2011, *MNRAS*, 418, 1346
- [ Lata S., Pandey A. K., Chen W. P., Maheswar G. and Chauhan N., 2012, *MNRAS*, 427, 1449
- [ Lata S., Pandey A. K., Panwar N. et al., 2016, *MNRAS*, 456, 2505
- [ Lata Sneh, Pandey Anil K., Kesh Yadav Ram, et al. 2019, *AJ*, 158, 68
- [ Lomb N. R., 1976, *Ap&SS*, 39, 447
- [ Littlefair S. P., Dhillon V. S., Martín E. L., 2005, *A&A*, 437, 637
- [ Meyer M. R., Calvet N., Hillenbrand L. A., 1997, *AJ*, 114, 288
- [ Mowlavi N., Barblan F., Saesen S., Eyer L., 2013, *A&A*, 554, 108
- [ Ostriker Eve C., Shu Frank H., 1995, *ApJ*, 447, 813
- [ Sato M. et al., 2008, *PASJ*, 60, 975
- [ Scholz A., Eislöffel J., Mundt R., 2009, *MNRAS*, 400, 1548
- [ Scargle J. D., 1982, *ApJ*, 263, 835
- [ Sesar B. et al, 2007, *AJ*, 134, 2236
- [ Sharma Saurabh, Pandey Anil K., Pandey Jeewan C., Chauhan Neelam, Ogura Katsuo, Ojha Devandra K., Borrissova Jura, Mito Hiroyuki, Verdugo Thomas, Bhatt Bhuwan C., 2012, *PASJ*, 64, 107
- [ Siess L., Dufour E., Forestini M., 2000, *A&A*, 358, 593
- [ Sinha Tirthendu, Sharma Saurabh, Pandey A. K., Yadav R. K., Ogura K., Matsunaga N., Kobayashi N., Bisht P. S., Pandey R., Ghosh A., 2020, *MNRAS*, 493, 267S
- [ Stetson P. B., 1987, *PASP*, 99, 191
- [ Stetson P. B., 1992, *J. R. Astron. Soc. Can.*, 86, 71
- [ Strom S. E., Strom K. M., Yost J., et al, 1972, *ApJ*, 173, L65
- [ Strom K. M., Strom S. E., Edwards S., Cabrit S., Skrutskie, M. F. 1989, *AJ*, 97, 1451
- [ Torres G., 2010, *AJ*, 140, 1158
- [ Waelkens C., 1991, *A&A*, 246, 453